J. Fluid Mech. (1971), *vol.* 49, *part* 3, *pp.* 417–449
Printed in Great Britain

Baroclinic annulus waves

By GARETH P. WILLIAMS

Geophysical Fluid Dynamics Laboratory/NOAA, Princeton University,
P.O. Box 308, Princeton, New Jersey 08540

(Received 4 January 1971)

The thermally driven motion of water contained in a rotating annulus of square cross-section and having a free surface is investigated by numerical integration of the three-dimensional non-linear Navier–Stokes equations. The nature of steady wave flow is examined in detail and a comparison made with the corresponding axisymmetric solution in parameter space.

The steady wave solution proves to be consistent kinematically, dynamically and energetically with Lorenz's hypothesis that the wave can be attributed to the baroclinic instability mechanism. The deviatoric† wave possesses some of the characteristics of the theoretical Eady wave and it is possible to define the complete deviatoric wave structure by means of two-dimensional quasi-phase, amplitude diagrams. These diagrams may also typify the nature of certain solutions to the non-separable baroclinic instability problem.

The wave motion is almost completely independent of the side boundary layers which make little contribution to the characteristics and energetics of the deviatoric flow. These side layers are approximately axisymmetric and appear qualitatively indistinguishable from their counterparts in the axisymmetric solution. However, significant Ekman layer features appear in the deviatoric wave structure.

Away from the boundaries the dynamical balance of terms is hydrostatic and quasi-geostrophic with changes of vertical vorticity influenced by stretching and viscous diffusion. Heat conduction is completely unimportant except in the side boundary layers.

The angular momentum transport by the deviatoric motion is largest at the free surface and is mainly against the angular momentum gradient. A strong outward deviatoric flux of momentum is found in the Ekman layer.

The dissipation of deviatoric kinetic energy occurs in the Ekman layer and jet whilst most of the dissipation of the mean kinetic energy occurs in the boundary layer of the inner wall.

The large differences between the axisymmetric and zonal mean states indicate that linear baroclinic instability analysis of the axisymmetric state is not strictly relevant to an understanding of the wave formation. The character of the wave suggests that the mean environment with which the deviatoric wave interacts is the *wave-present* zonal mean state. Only a non-linear finite amplitude baroclinic instability analysis (as yet undeveloped) could possibly explain the wave formation.

† The deviation from the zonal mean.

1. Introduction

The object of this paper is to examine the nature of the steady waves that occur in the annulus experiments. This will be done by analyzing a numerical solution of the Navier–Stokes equations. The solution was first outlined in an earlier paper on the integration technique (Williams 1969).

The motivation for studying annulus convection has been discussed by Lorenz (1967). The main reason for study is the apparent relevance of the experiments to baroclinic instability theory and thence to various large scale phenomena such as the general circulation of the atmosphere.

The present results will support the explanation of the various annulus modes first proposed by Lorenz (1953). In his article he made 3 major hypotheses which have some bearing on the problem in hand: (i) that symmetric flow is mathematically possible but physically unstable in the wave régime; (ii) that the disturbances leading to the waves gain their kinetic energy from existing potential energy rather than existing kinetic energy, i.e. they are a baroclinically unstable flow; (iii) that heating and rotation both affect the régime of flow by affecting the static stability parameter. Some of the consequences of these hypotheses were later examined by Lorenz (1962, 1963).

A numerical solution for an annulus wave was obtained to try to determine the complete nature of such waves and thereby test the validity of Lorenz's hypotheses. Having established the deviatoric flow to be essentially a form of finite amplitude Eady wave, we then discuss the energy, momentum and heat transport characteristics of such a wave. We also investigate how active the different boundary layers are in the mechanics of the wave and how the phase-amplitude characteristics of linearized theory are modified in our steady finite amplitude wave with its more complex underlying basic fields. Pedlosky (1970) has recently instigated the analytic study of finite amplitude baroclinic waves.

On the geophysical side, the role of baroclinic instability in producing the atmospheric cyclone–anticyclone systems and the possible transfer properties of such systems in the global circulation has most recently been discussed by Pedlosky (1964) and Green (1970). We will also use our results as evidence in support of the view that many of the characteristic features of the atmosphere's dynamics and energetics simply reflect the finite amplitude consequences of baroclinic instability.

Not all the details of the solution are presented in this paper. Certain synoptic aspects are presented in a companion paper (Williams 1971), to which occasional reference will be made.

2. The fundamental equations

We will consider the motion of a fluid bounded by two co-axial cylinders of inner and outer radii a, b respectively, and two parallel horizontal planes which are a distance d apart, figure 1 (a). The container rotates at a uniform rate $\mathbf{\Omega}$, where the rotation vector, anti-parallel to gravity $\mathbf{g}$, coincides with the vertical axis of the cylinders. Motion relative to the solid rotation of the container is

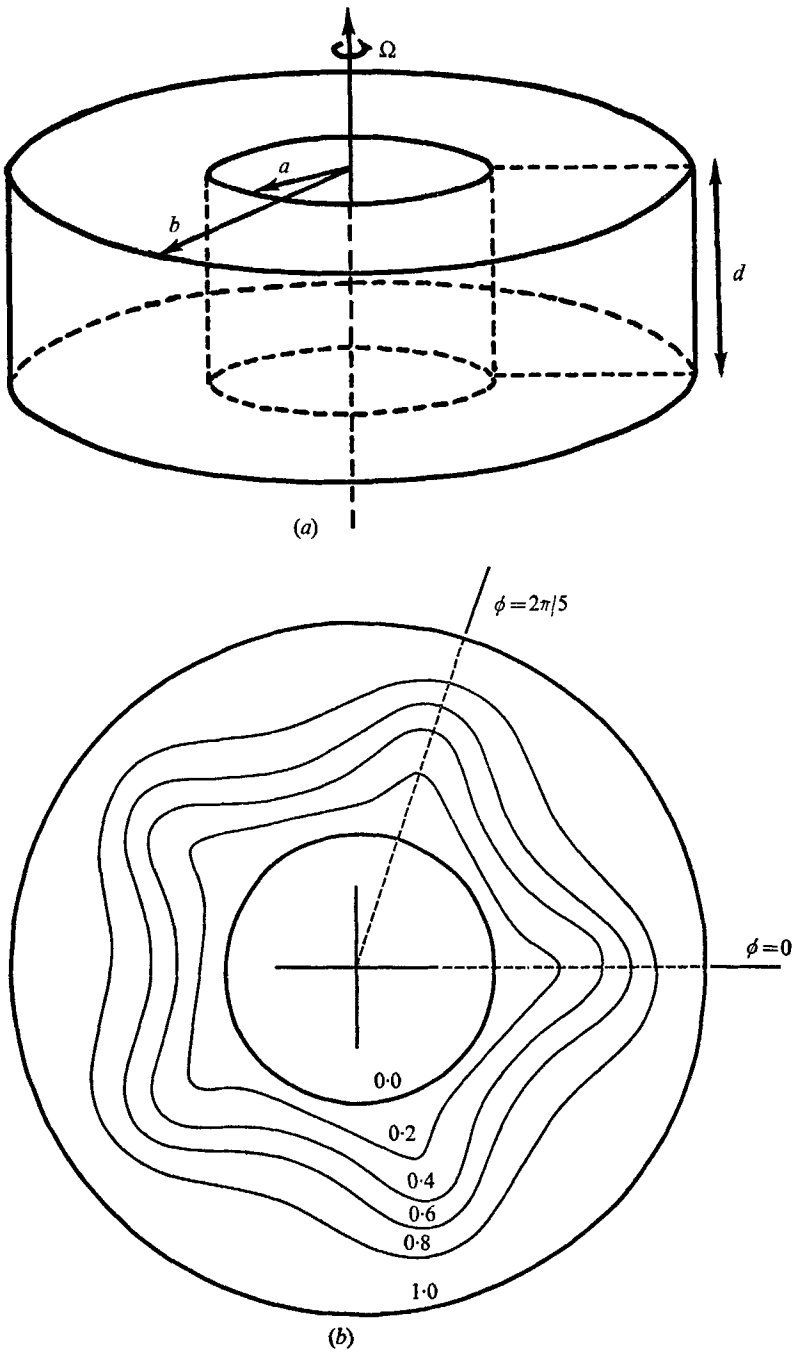

FIGURE 1. (*a*) Configuration of the system (close to actual size). (*b*) Pressure wave at upper surface. Container rotates counterclockwise at $\Omega = 0{\cdot}8$ rad sec^{-1} and the wave rotates counter-clockwise relative to the container at $\Omega^* = 0{\cdot}033$ rad sec^{-1}. Domain of interest is $\phi = 0°$ to 72°. The pressure is normalized in terms of the maximum and minimum values which are 1·8319 and 0·6974 cm^2 sec^{-2}.

measured in cylindrical co-ordinates r, ϕ, z based on the axis, r being radial and z vertical. The velocity components are u, v, w in the zonal, radial and vertical directions respectively. The angular size of the annulus sector Φ is normally 2π but for the solution we consider only the sector $\Phi = 2\pi/5$, figure 1 (b).

The following definition of a Boussinesq liquid is taken for convenience: that density variations are negligible except in the buoyancy term and that the coefficients ν, κ, β of viscosity, heat diffusivity and thermal expansion are constant. We also take the centrifugal acceleration to be negligible compared with gravity: $\Omega^2 b/g \ll 1$, as a consequence of which the upper surface can be taken to be of constant height and the free-slip rigid lid condition can be used for this surface.

The perfectly conducting inner and outer cylinders are held at different constant temperatures T_a and T_b respectively. This imposed horizontal temperature differential $\Delta T = T_b - T_a$ drives the fluid away from a state of solid rotation. The base and upper surface are thermally insulating.

Upon writing the hydrostatic pressure deviation as $\pi = p/\rho_0$ and the temperature deviation from T_a as T, the Navier–Stokes equations for this system may be expressed in the following form:

$$\frac{Dv}{Dt} = -\pi_r + \left(2\Omega + \frac{u}{r}\right) u + \nu\left(\nabla^2 v - \frac{v}{r^2} - \frac{2u_\phi}{r^2}\right), \tag{1}$$

$$\frac{Du}{Dt} = -\frac{1}{r}\pi_\phi - \left(2\Omega + \frac{u}{r}\right) v + \nu\left(\nabla^2 u + 2\frac{v_\phi}{r^2} - \frac{u}{r^2}\right), \tag{2}$$

$$\frac{Dw}{Dt} = -\pi_z + \beta g T + \nu\nabla^2 w, \tag{3}$$

with the heat transfer equation as

$$DT/Dt = \kappa\nabla^2 T, \tag{4}$$

and the equation of mass conservation as

$$(rv)_r + u_\phi + r w_z = 0, \tag{5}$$

where we have defined the operator identities

$$\frac{Dq}{Dt} \equiv q_t + v q_r + \frac{u}{r} q_\phi + w q_z, \tag{6}$$

$$\nabla^2 q \equiv q_{rr} + \frac{1}{r} q_r + \frac{1}{r^2} q_{\phi\phi} + q_{zz}. \tag{7}$$

The boundary conditions as used in the calculations and which express the state of the fluid at the boundaries are:

(i) on the base

$$w = v = u = T_z = 0, \quad \pi_z = \beta g T + \nu w_{zz}; \tag{8}$$

(ii) on the free surface

$$w = v_z = u_z = T_z = 0, \quad \pi_z = \beta g T; \tag{9}$$

(iii) on the side walls

$$w = v = u = 0, \quad \pi_r = \nu\left(v_{rr} + \frac{v_r}{r}\right); \tag{10}$$

and $T = 0$, ΔT applied at $r = a, b$ respectively.

The procedure for solving the system of equations (1)–(10) involves extensive numerical calculation. The method has been documented elsewhere (Williams 1969), and the reader is referred to that paper for further details. In brief, the method consists of representing the equations in a carefully chosen finite difference form and programming the calculation for a computer. We can then obtain solutions to the above equations as functions of space and time.

3. The analysis equations

In discussing the maintenance and the transfer properties of the annulus wave we find it informative to calculate the elements of the following set of energy, angular momentum and heat equations. Furthermore, it is useful to look at the solution in terms of the zonal (i.e. azimuthal) average and deviations therefrom for certain quantities. This procedure is justified *a posteriori* by the ensuing simplification and insight achieved. We use the term 'deviatoric' for the zonal deviation rather than 'eddy' or 'perturbation' as the flow is laminar and finite amplitude. The following averaging operators will be used (i) the zonal

$$\overline{(\,)} = \frac{1}{\Phi}\int_0^{\Phi}(\,)\,d\phi,$$

(ii) the vertical

$$\overline{(\,)}^{V} = \frac{1}{d}\int_0^{d}(\,)\,dz$$

and (iii) the radial

$$\overline{(\,)}^{H} = \int_a^b(\,)\,r\,dr \Big/ \int_a^b r\,dr.$$

Primed quantities denote deviations from the zonal mean.

(*a*) *The kinetic energy*

Writing the total squared velocity as $c^2 = u^2 + v^2 + w^2$ we define the total kinetic energy as $K_T = \frac{1}{2}c^2$ and the zonal mean and deviatoric energies as $K_z = \frac{1}{2}\bar{c}^2$ and $K_E = K_T - K_z$ respectively. Defining the deviatoric energy this way produces locally consistent transfer equations, with identifiable conversions and interactions, see Smagorinsky, Manabe & Holloway (1965).

(*b*) *The global energy transfers*

To discuss the net energy transfers between the potential and kinetic forms we have the equations:

$$\frac{\partial}{\partial t}\langle K_z\rangle = +\langle\mathscr{C}(K_E, K_z)\rangle + \langle\beta g\overline{w}\overline{T}\rangle + \nu\langle\overline{\mathbf{v}}.\overline{\mathbf{F}}\rangle, \tag{11}$$

$$\frac{\partial}{\partial t}\langle K_E\rangle = -\langle\mathscr{C}(K_E, K_z)\rangle + \langle\beta g\overline{w'T'}\rangle + \nu\langle\overline{\mathbf{v}'.\mathbf{F}'}\rangle, \tag{12}$$

$$\frac{\partial}{\partial t}\langle P\rangle = -\langle\beta g\overline{w}\overline{T}\rangle - \langle\beta g\overline{w'T'}\rangle - \beta g\kappa\langle z\nabla^2 T\rangle, \tag{13}$$

where $\langle\ \rangle$ denotes integration (not averaging) over the whole annular sector. The potential energy has been defined as $P = (-\beta g z T)$ and $\mathbf{v}.\mathbf{F}$ is used to represent the friction terms. The term $\mathscr{C}(K_E, K_z)$ represents the net conversion of one kinetic energy form into the other. Another associated term $\mathscr{I}(K_E, K_z)$ in equations (16)–(19) represents a local interaction between the two kinetic energies that produces no net exchange. The full local form of these conversion and interaction terms is

$$\begin{aligned}\mathscr{C}(K_E, K_z) \equiv &+[(\overline{w'u'})\,\overline{u}_z + r(\overline{v'u'})\,(\overline{u}/r)_r] + [(\overline{v'w'})\,\overline{v}_z + (\overline{v'v'})\,\overline{v}_r] \\ &+[(\overline{w'w'})\,\overline{w}_z + (\overline{v'w'})\,\overline{w}_r] + [\overline{v}/r(\overline{u'u'})],\end{aligned} \tag{14}$$

$$\begin{aligned}\mathscr{I}(K_E, K_z) \equiv &-(1/r)\,[r(\overline{u}(\overline{v'u'}) + \overline{v}(\overline{v'v'}) + \overline{w}(\overline{v'w'}))]_r \\ &-[\overline{u}(\overline{w'u'}) + \overline{v}(\overline{w'v'}) + \overline{w}(\overline{w'w'})]_z.\end{aligned} \tag{15}$$

(c) The vertical kinetic energy transfer equations

To examine the interaction between different levels of the flow, particularly between the Ekman layer and the interior, we construct the radial, zonal average of the kinetic energy equations. The resulting expressions, functions of z only, describe the transfer of energy in the vertical.

$$\begin{aligned}\frac{\partial}{\partial t}\overline{\overline{K}}^H_z = &-\overline{\overline{(w\overline{K}_z)}}^H_z - \overline{\overline{(\overline{w}\overline{\overline{u}})}}^H_z + \overline{\overline{\mathscr{C}}}^H(K_E, K_z) + \overline{\overline{\mathscr{I}}}^H(K_E, K_z) \\ &+\beta g\overline{\overline{(\overline{w}\overline{T})}}^H + \nu\overline{\overline{(\overline{\mathbf{v}}.\overline{\mathbf{F}})}}^H,\end{aligned} \tag{16}$$

$$\begin{aligned}\frac{\partial}{\partial t}\overline{\overline{K}}^H_E = &-\overline{\overline{(w\overline{K}_E)}}^H_z - \overline{\overline{(w'\pi')}}^H_z - \overline{\overline{\mathscr{C}}}^H(K_E, K_z) - \overline{\overline{\mathscr{I}}}^H(K_E, K_z) \\ &+\beta g\overline{\overline{(w'T')}}^H + \nu\overline{\overline{(\mathbf{v}'.\mathbf{F}')}}^H.\end{aligned} \tag{17}$$

The above equations are in a desirable D/Dt form. Terms represent energy changes by convective transfer, pressure interaction, non-linear exchanges, conversion of potential energy by buoyancy forces and frictional dissipation.

(d) The radial kinetic energy transfer equations

As a measure of the overall radial transfer of energy and the interaction between the side boundary layers and the interior, we define the kinetic energy equations as functions of r only. These are:

$$\begin{aligned}\frac{\partial}{\partial t}\overline{\overline{K}}^V_z = &-\frac{1}{r}\overline{\overline{(rv\overline{K}_z)}}^V_r - \frac{1}{r}\overline{\overline{(r\overline{v}\overline{\overline{u}})}}^V_r + \overline{\overline{\mathscr{C}}}^V(K_E, K_z) + \overline{\overline{\mathscr{I}}}^V(K_E, K_z) \\ &+\beta g\overline{\overline{(\overline{w}\overline{T})}}^V + \nu\overline{\overline{(\overline{\mathbf{v}}.\overline{\mathbf{F}})}}^V,\end{aligned} \tag{18}$$

$$\begin{aligned}\frac{\partial}{\partial t}\overline{\overline{K}}^V_E = &-\frac{1}{r}\overline{\overline{(rv\overline{K}_E)}}^V_r - \frac{1}{r}\overline{\overline{(rv'\pi')}}^V_r - \overline{\overline{\mathscr{C}}}^V(K_E, K_z) - \overline{\overline{\mathscr{I}}}^V(K_E, K_z) \\ &+\beta g\overline{\overline{(w'T')}}^V + \nu\overline{\overline{(\mathbf{v}'.\mathbf{F}')}}^V.\end{aligned} \tag{19}$$

When the radial variation of these terms is presented later in figure 16 they will be multiplied by r so that the contributions to the net global integrals can be judged.

(*e*) *Local variation of energy dissipation*

So that we may discuss the local variations of the sources and sinks of kinetic energy the molecular transform function must first be written in tensor notation as

$$\nu u_i \frac{\partial^2 u_i}{\partial x_j^2} = \nu\left[\frac{\partial^2}{\partial x_j^2}(\tfrac{1}{2}u_i^2) + \frac{\partial^2}{\partial x_i \partial x_j}(u_i u_j)\right] - \epsilon^2, \tag{20}$$

$$\epsilon^2 = \tfrac{1}{2}\nu\left(\frac{\partial u_i}{\partial x_j} + \frac{\partial u_j}{\partial x_i}\right)^2. \tag{21}$$

The first term on the right of equation (20) is the general energy diffusion (zero volume integral). The quantity ϵ^2 is an invariant and is the dissipation of energy. In cylindrical co-ordinates ϵ^2 may be written in terms of the rate of strain functions:

$$\epsilon^2 = \tfrac{1}{2}\nu[e_{rr}^2 + e_{\phi\phi}^2 + e_{zz}^2 + 2e_{\phi z}^2 + 2e_{zr}^2 + 2e_{r\phi}^2], \tag{22}$$

where

$$\left.\begin{aligned} &e_{rr} = 2v_r; \quad e_{\phi\phi} = \frac{2}{r}(u_\phi + v); \quad e_{zz} = 2w_z; \\ &e_{\phi z} = \frac{w_\phi}{r} + u_z; \quad e_{rz} = v_z + w_r; \quad e_{r\phi} = \frac{v_\phi}{r} + u_r - \frac{u}{r}. \end{aligned}\right\} \tag{23}$$

This dissipation function can be divided into zonal mean and deviatoric components $\bar{\epsilon}^2$ and $\overline{\epsilon'^2}$. These are calculated.

(*f*) *The angular momentum transfers*

The angular momentum $m = r(u + \Omega r)$ is a fundamental entity in rotating fluids even though it may not be a conserved quantity. The basic equation for the zonal mean angular momentum is

$$\bar{m}_t = -[\bar{v}\bar{m}_r + \bar{w}\bar{m}_z] - [(1/r)(\overline{rv'm'})_r + (\overline{w'm'})_z] + \nu[r(\bar{m}_r/r)_r + \bar{m}_{zz}]. \tag{24}$$

Two useful integral forms of this equation are the vertical mean form and the transport form for the balance of an inner ring. These have equations

$$\overline{\bar{m}}_t^V = -\left[\frac{1}{r}\overline{(r\bar{v}\bar{m})_r}^V\right] - \left[\frac{1}{r}\overline{(\overline{rv'm'})_r}^V\right] + \nu\left[r\left(\frac{\overline{\bar{m}_r}^V}{r}\right)_r - (\bar{m}_z)_{\text{at } z=0}\right], \tag{25}$$

and

$$\begin{aligned}\int_a^r\int_0^d \bar{m}_t\, r\, dr\, dz = &-\left[\int_0^d r\bar{v}\bar{m}\, dz\right]_{\text{at } r} - \left[\int_0^d r\overline{v'm'}\, d_z\right]_{\text{at } r} - \nu\left[\int_a^r r^2\bar{u}_z\, dr\right]_{\text{at } z=0} \\ &+ \nu\left[\int_0^d r^3\left(\frac{\bar{u}}{r}\right)_r dz\right]_{\text{at } r} - \nu\left[\int_0^d r^3\left(\frac{\bar{u}}{r}\right)_r dz\right]_{\text{at } r=a}.\end{aligned} \tag{26}$$

Equation (25) provides a useful estimate of the overall contribution of the different mechanisms to the angular momentum balance at different radii whereas (26) demonstrates more clearly how inner regions have their angular momentum maintained.

(g) The heat transfer

The following equation for the zonal mean temperature provides a measure of how the heat transfer depends on the various mechanisms:

$$\overline{T}_t = -[\overline{v}\overline{T}_r + \overline{w}\overline{T}_z] - [1/r(r\overline{v'T'})_r + (\overline{w'T'})_z] + \kappa\nabla^2\overline{T}. \tag{27}$$

As a measure of the effectiveness of the flow as a heat transferring mechanism we define a Nusselt number for each sidewall

$$Nu(c) = \frac{c}{d}\log\frac{b}{a}\int_0^d \frac{\overline{T}_r(c)}{\Delta T}\,dz, \quad c = a, b, \tag{28}$$

relative to the amount of heat that would be transferred by solid conduction under the same ΔT.

The computation of the elements of (11) to (28) involves a programming effort comparable to that for the prediction equations.

4. Parameter values and preliminary exploration of parameter space

The following parameter values were chosen as being suitable for a calculation to produce a steady wave.

(i) Geometry: $a = 2\,\text{cm}$, $b = 5\,\text{cm}$, $d = 3\,\text{cm}$.

(ii) Physical parameters of water at 20 °C:

$$\nu = 1{\cdot}008 \times 10^{-2}\,\text{cm}^2\,\text{sec}^{-1}, \quad \kappa = 1{\cdot}420 \times 10^{-3}\,\text{cm}^2\,\text{sec}^{-1},$$
$$\beta = 2{\cdot}054 \times 10^{-4}\,(^\circ\text{C})^{-1}.$$

(iii) $\Delta T = 5\,^\circ\text{C}$, $T_0 = 20\,^\circ\text{C}$, $\Omega = 0{\cdot}8\,\text{rad}\,\text{sec}^{-1}$, $g = 981\,\text{cm}\,\text{sec}^{-2}$.

(iv) Resolution: $\Delta r' = \frac{1}{32}$, $\Delta z' = \frac{1}{32}$, $\Delta\phi' = \frac{1}{36}$.

(v) Non-dimensional numbers of solution:

Thermal Rossby number, $\pi_4 \equiv \beta g \Delta T d/\Omega^2(b-a)^2 = 0{\cdot}525$;‡

Taylor number, $\pi_5 \equiv 4\Omega^2(b-a)^5/\nu^2 d = 2{\cdot}041 \times 10^6$;

Dynamic Rossby numbers, $R_0 \equiv u_{\max}/2\Omega(b-a) = 0{\cdot}108$† for wave solution $= 0{\cdot}062$‡ for axisymmetric solution;

Nusselt number, $Nu = 7{\cdot}3$, $3{\cdot}24$† for wave and axisymmetric solutions.

(vi) Wave rotation rate $\Omega^* = 0{\cdot}033$†$(\doteqdot \Omega/24)$. Time iteration involved 10 000 steps at $\Delta t = 0{\cdot}05\,\text{sec}$.

This set of parameters was chosen as it satisfied three criteria: (i) that the geometry be non-extreme and close to the range of laboratory values, (ii) that the boundary layers not be too thin and hence be accurately resolvable and (iii) that ΔT, Ω should not have too large a range in traversing the various régimes.

The transition spectrum for the parameter values as estimated from observational data is shown in figure 2. The boundary for the transition from wave flow to irregular flow is unknown. Calculations were made along the line $\Delta T = 5^\circ\,\text{C}$. Traversing this line we can pass from axisymmetric flow at point A ($\Omega = 0{\cdot}5\,\text{rad}\,\text{sec}^{-1}$) to wave flow, then to irregular flow near point C ($\Omega = 2{\cdot}0\,\text{rad}\,\text{sec}^{-1}$). For

† $\pi 4/4$ would be a better Rossby number.
‡ Values given by solution.

the parameter values of points A to C the boundary layers can be adequately resolved and thus this parameter domain is suitable for obtaining numerical solutions for any régime of flow. (However, the vacillating flows have only weak amplitudes and are not satisfactory for further study.)

Using medium resolution, a preliminary set of calculations was made at various points along the line AC. These calculations confirmed that the transition curve between axisymmetric and wave flow lay near the D, $\Omega = 0{\cdot}6\,\mathrm{rad\,sec^{-1}}$, point. They also established that beyond C the flows tended to be irregular. The wave-numbers ranged from 4 to 6 between D and C as observations suggested. Point H, $\Omega = 0{\cdot}8\,\mathrm{rad\,sec^{-1}}$, was chosen for the detailed calculations as it seemed to be a point with a high possibility of producing a steady wave.

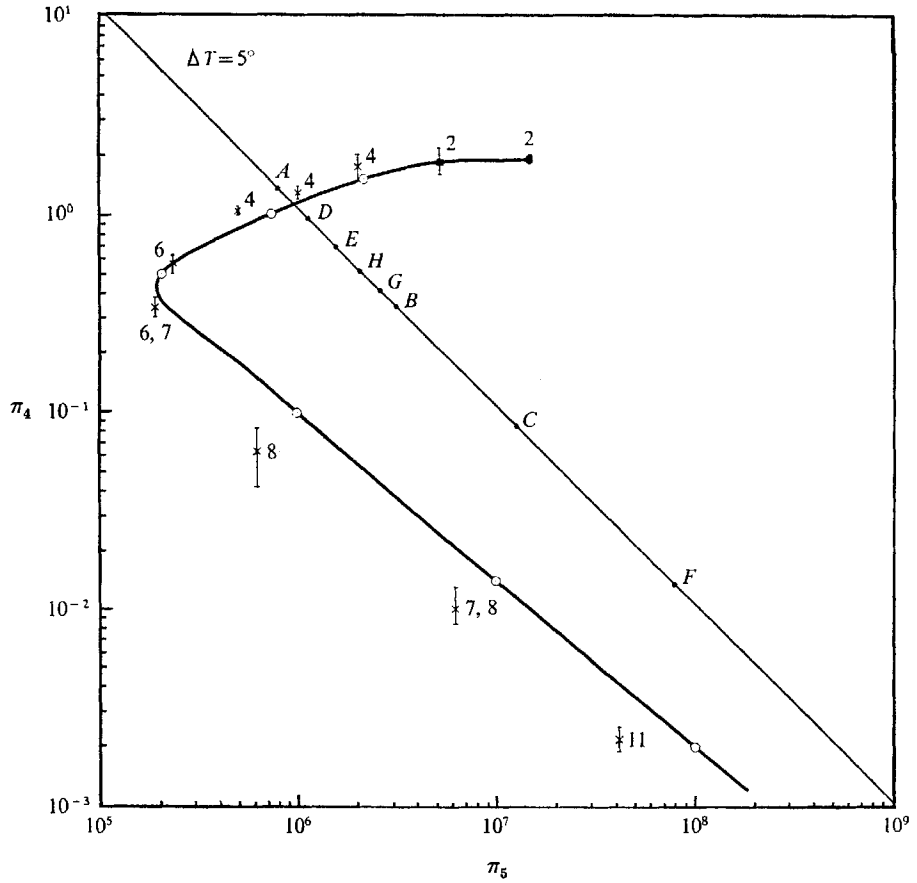

FIGURE 2. Transition curve between axisymmetric motion (to the left) and wave motion constructed from data of Fowlis & Hide (1965) for the parameters of the calculation. Co-ordinates are the thermal Rossby π_4 and Taylor π_5 numbers. Circled values come from the summary curves of Fowlis & Hide interpreted for our parameter values. Cross marks indicate transition points for observations with small fluid depth (5 cm) and square marks are likewise for small inner radius. Associated wave-numbers are given as a guide. The diagonal line $\Delta T = 5°$ C is locus of interest. The solution is obtained at H ($\Omega = 0{\cdot}8$). Other points on the line have values of Ω, $A = 0{\cdot}5$, $D = 0{\cdot}6$, $E = 0{\cdot}7$, $H = 0{\cdot}8$, $G = 0{\cdot}9$, $B = 1{\cdot}0$, $C = 2{\cdot}0$, $F = 5{\cdot}0$. The symmetric to wave transition occurs near $\Omega = 0{\cdot}55$ and irregular flow occurs near point C.

A numerical resolution of 34 by 34 points was decided upon for the vertical and radial directions. The accuracy of this resolution was tested and confirmed by comparing the axisymmetric solution with that for a 48×48 resolution and by comparing numerical and analytical Ekman layers for the axisymmetric flow, see Williams (1971) for further details. So that the resolution in the azimuthal direction would be optimum and comparable with the radial resolution, the calculations were confined to one wavelength. Having determined that wave-number 5 occurs at these parameter values over the 2π sector, the calculations were carried out for a sector of $\Phi = 2\pi/5$ with a resolution of 38 points.

5. Time development

The time development of the flow is illustrated in figure 3 in terms of global integrals. At time $t = 0$ the initial state of the fluid is one of solid rotation $\mathbf{v} = 0$ and isothermal temperature $T = \frac{1}{2}\Delta T$. With a time step of 0·05 sec integration of equations (1) to (10) was made until a quasi-steady wave motion at 517 sec was achieved.

For the first 150 sec the flow remains axisymmetric as the monotonic curves show. A small random temperature disturbance was added at 50 sec so that when the fluid became unstable at 150 sec a full three-dimensional motion grew. The growth of the wave is indicated by the deviatoric kinetic energy quantity $\langle \frac{1}{2}u'^2 \rangle$. As the wave begins to develop the conversion of potential to kinetic energy is abruptly increased. The other integrals show similar growth patterns although the zonal mean kinetic energy quantity $\langle \frac{1}{2}\overline{u}^2 \rangle$ decreases during the wave initiation stage. The sudden wave growth halts near 200 sec and declines, to level off at 230 sec. Thereafter the flow tends to a steadiness at 500 sec where the wave is fully developed, in equilibrium and rotating uniformly relative to the container at a rate of $\Omega^* = 0{\cdot}033$ rad sec^{-1}.

For convenience the solution at 517 sec will be discussed, this time being the time when the trough of the upper surface pressure wave is in the $\phi' = 0$ position. The solution outlined by Williams (1969) was at the 400 sec stage and differs slightly from that in this paper.

The average temperature of the water changes from $0{\cdot}5\Delta T$ to approximately $\frac{2}{3}\Delta T$ during the calculation. This explains the non-constancy of the total energy in figure 3.

6. Comparison of axisymmetric and zonal mean solutions

In this section we discuss only the zonally averaged fields of the wave solution, reserving consideration of the deviatoric characteristics for the next two sections.

Figure 4 contains the zonal mean basic fields of the wave solution together with the axisymmetric solution for the same parameter values (point H). The features of the axisymmetric solution resemble those obtained in earlier studies (Williams 1967). The radial flows form a single cell and triple cell system in the axisymmetric and wave solutions respectively, with stronger velocities occurring in the wave case. The maximum zonal velocity ('jet') is larger for the symmetric flow, 0·52 cm sec^{-1}, than for the mean wave flow, 0·30 cm sec^{-1}, although

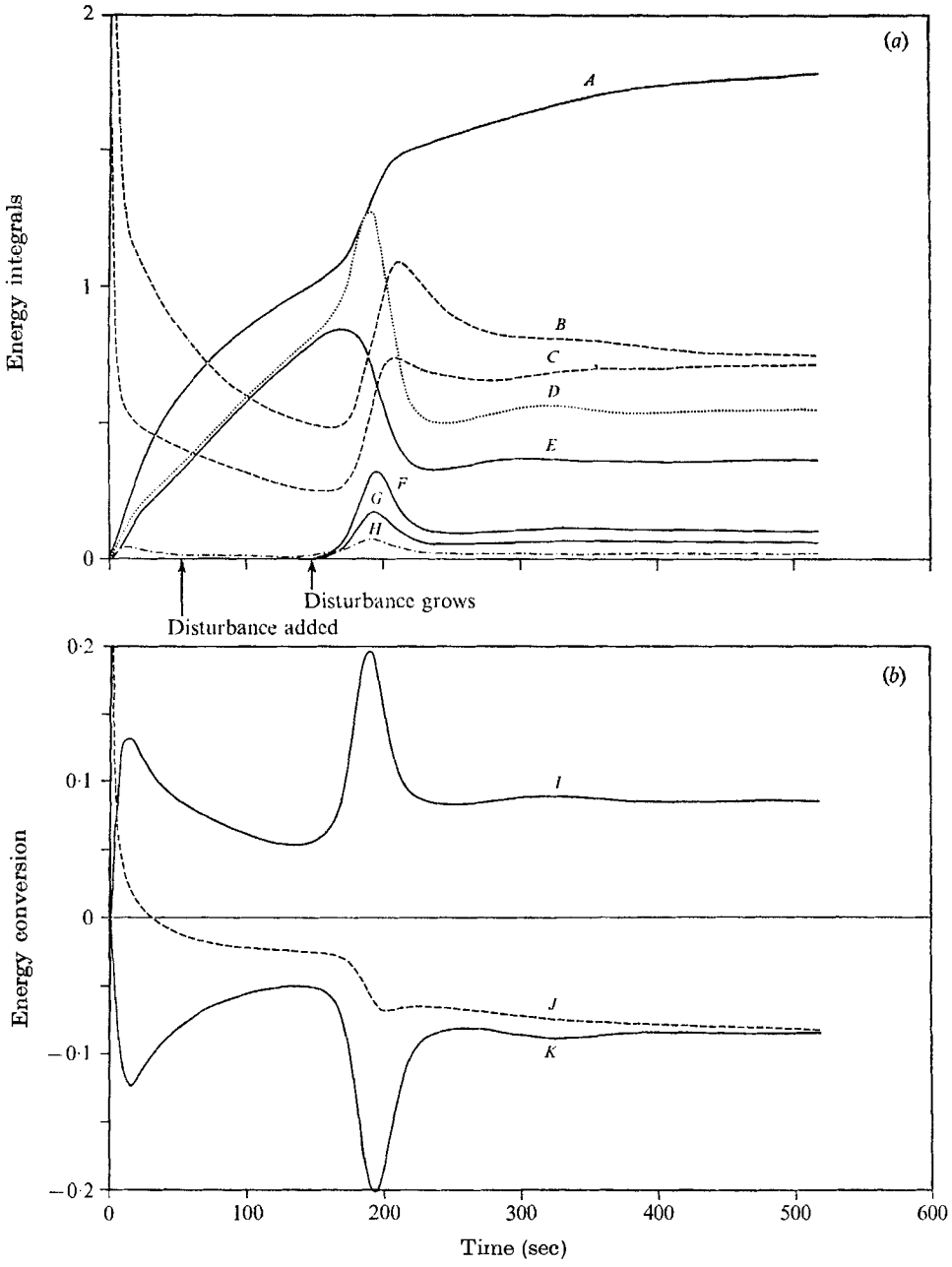

FIGURE 3. Time development of the calculation as given by integral quantities. Wave develops from axisymmetric flow at 150 sec and reaches quasi-steady state at 500 sec. Time step was 0·05 sec for 10,000 steps. Diagram (*a*) has the total quantities (*A*) $10^{-1}\times(-P-30)$; (*B*) $10^{-1}\times Nu(b)$; (*C*) $10^{-1}\times Nu(a)$; (*D*) $\langle\frac{1}{2}c^2\rangle$; (*E*) $\langle\frac{1}{2}\overline{u}^2\rangle$; (*F*) $\langle\frac{1}{2}v^2\rangle$; (*G*) $\langle\frac{1}{2}u'^2\rangle$; (*H*) $\langle\frac{1}{2}w^2\rangle$. Diagram (*b*) has energy conversions (*I*) $\langle\beta gwT\rangle$; (*J*) $\beta g\kappa\langle z\nabla^2T\rangle$; (*K*) $\nu\langle\mathbf{v}.\mathbf{F}\rangle$, from equation (13). In c.g.s. units.

the local jet reaches 0·52 cm sec^{-1} in the trough of the wave. Because of strong curvature effects in this geometry the relative angular momentum is also given, in figure 4(*c*), and this shows that the zonal mean field $r\bar{u}$ has a vertical axis and a degree of symmetry about $r' = \frac{1}{2}$ not exhibited by $\bar{u}$. Figure 5 for the averaged profiles of zonal velocity shows a similarity in overall character for the two cases.

Stronger thermal boundary layers form on the sidewalls in the wave case and the isotherms lie more horizontal, resulting in a larger static stability, figures 4 and 6. In the vertical profile of mean temperature, figure 6(*b*), the variation goes as $z'^{\frac{1}{2}}$ away from the horizontal boundaries. The global mean normalized

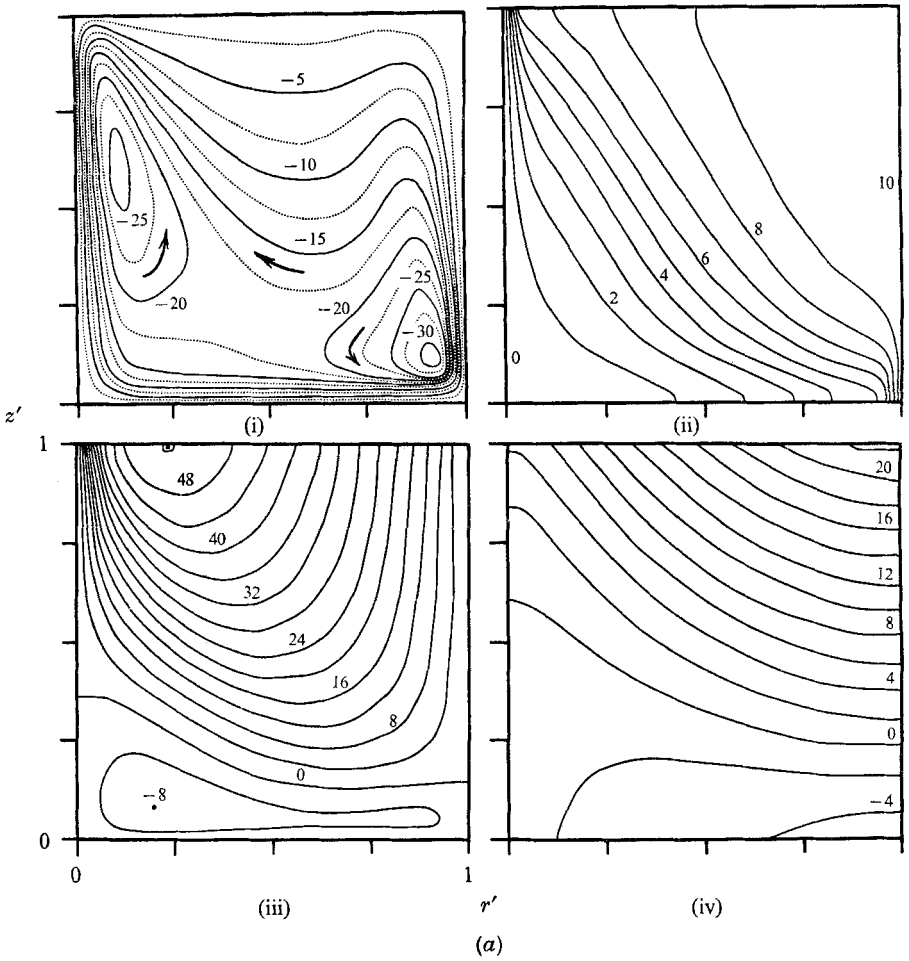

(*a*)

FIGURE 4. (*a*) Vertical sections of the steady state axisymmetric solution at the same physical parameters as the wave solution. (i) ($\psi \times 10^3$) cm sec^{-1}, (ii) ($T/\Delta T \times 10$), (iii) ($u \times 10^2$) cm sec^{-1}, (iv) ($\pi \times 10^1$) cm^2 sec^{-2}. Nusselt number is 3·24. Cold inner wall is on the left of each diagram. Co-ordinates all as in (iii).

(*b*) Vertical sections of zonally averaged fields of the steady state wave solution. (i) $\overline{\psi} \times 10^3$) cm^3 sec^{-1}, (ii) ($\overline{T}/\Delta T \times 10$), (iii) ($\overline{u} \times 10^2$) cm sec^{-1}, (iv) ($\overline{\pi} \times 10^1$) cm^2 sec^{-2}. The stream function is defined by $r\bar{v} = -\overline{\psi}_z$; $r\overline{w} = \overline{\psi}_r$.

(*c*) Relative angular momentum ru for (i) axisymmetric and (ii) zonally averaged wave solutions, in cm^2 sec^{-1}.

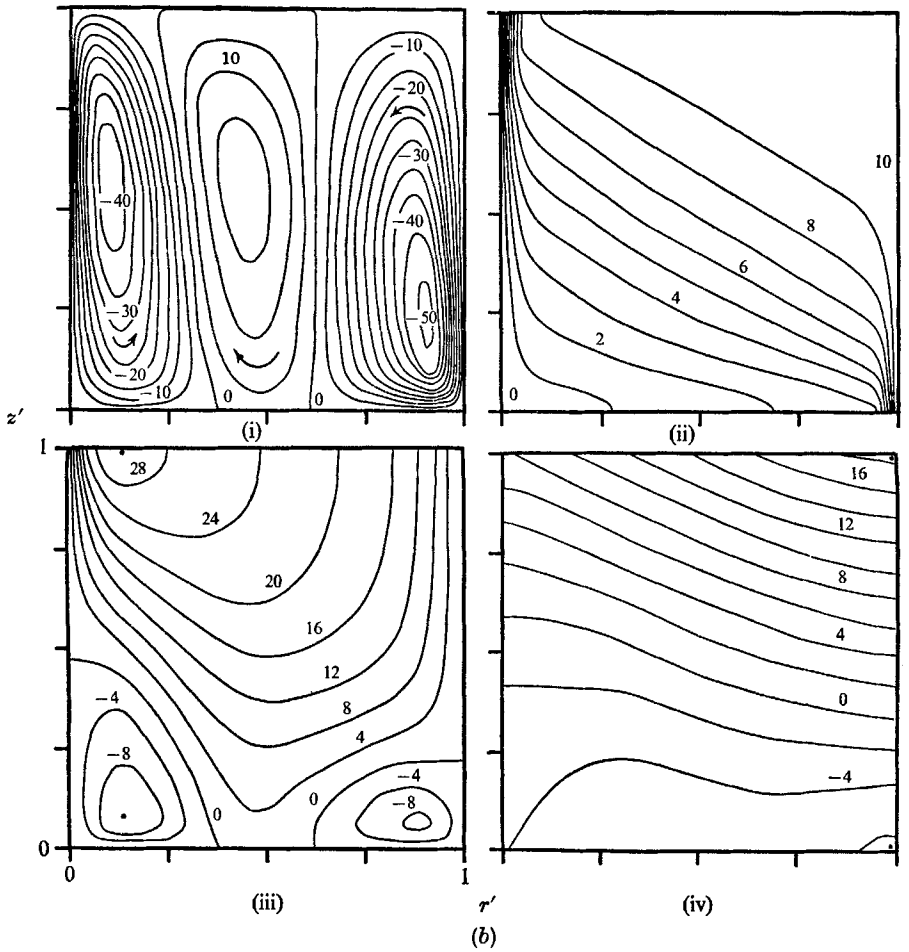

For legend see facing page.

temperatures are 0·670 and 0·672 for the wave and symmetric cases respectively. These values are close to the $\frac{2}{3}$ value for $z'^{\frac{1}{2}}$. Whilst the parabolic behaviour of $\overline{T}$ is not complete and may be fortuitous clearly the variation of $\overline{T}$ with z is not linear. We might speculate that this parabolic temperature surface perhaps indicates what variation temperature surfaces with minimum available potential energy will have. Because of thermal boundary layering the temperature differential across the interior, $\Delta_I \overline{T}$, varies strongly with height, figure 6 (*b*), reaching a maximum near $z' = \frac{1}{3}$. In fact there is a significant variation in the interior baroclinicity, $\overline{T}_{r'}$, which has a diagonal axis, figure 7. Thus we see deviations in both the axisymmetric and wave fields from the simple basic fields assumed in linear theories.

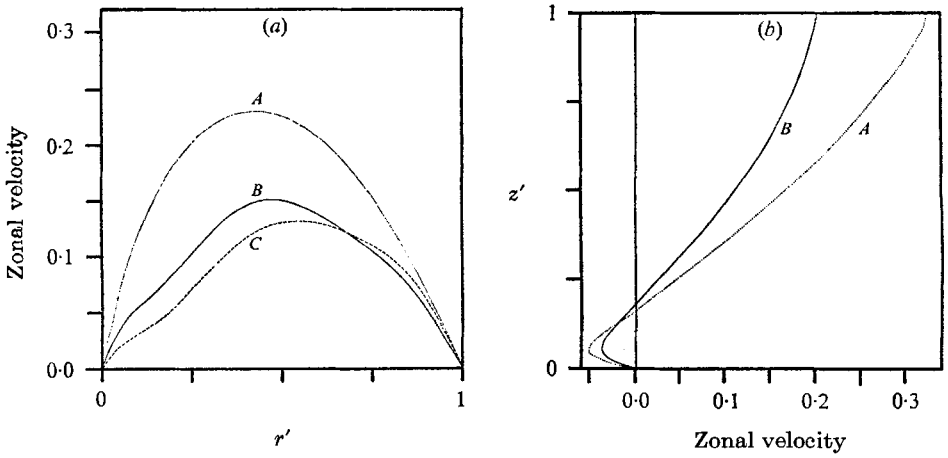

FIGURE 5. Zonal velocity profiles. (*a*) Vertically averaged profiles of (*A*) axisymmetric u, (*B*) wave $\overline{u}$ and (*C*) scaled-wave angular momentum $\frac{1}{4}r\overline{u}$. (*b*) Radially averaged profiles of (*A*) axisymmetric u and (*B*) wave $\overline{u}$, in cm sec^{-1}.

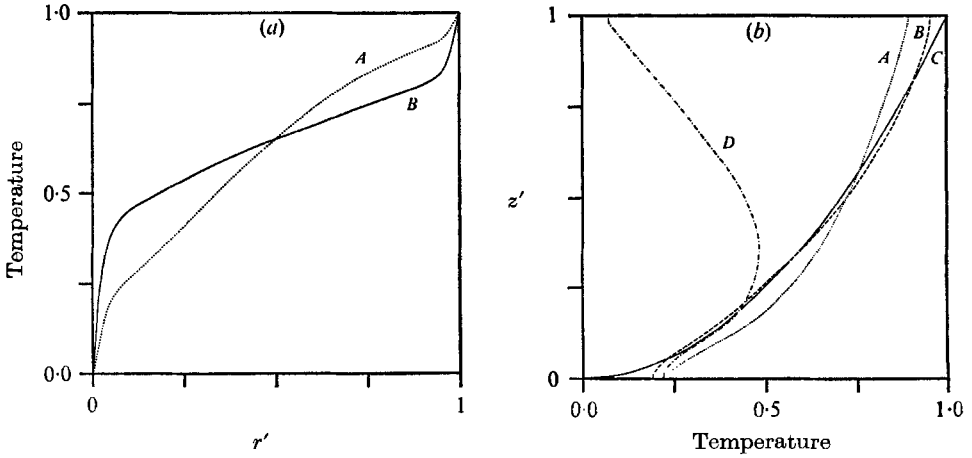

FIGURE 6. Temperature profiles. (*a*) Vertically averaged profile of $\overline{T}/\Delta T$ for (*A*) axisymmetric (*B*) wave mean. (*b*) Radially averaged profile of $\overline{T}/\Delta T$ for (*A*) axisymmetric, (*B*) wave mean, (*C*) is $(z/d)^{\frac{1}{2}}$ and (*D*) is the temperature differential across the interior of the fluid, $\Delta_I \overline{T}/\Delta T$, where $\Delta_I \overline{T} = \{\overline{T}$ at $r' = \frac{57}{64}$ minus $\overline{T}$ at $r' = \frac{7}{64}\}$. Mean temperatures are 0·672, 0·670 for axisymmetric and wave solutions.

The dynamics of the above type of axisymmetric flow has been discussed by Williams (1967) while McIntyre (1968) has analyzed the closely related rigid lid system. Primarily the convective side boundary layers drive the axisymmetric flow. These boundary layers produce an interior temperature field to which the zonal velocity responds through the thermal wind equation. Small interior meridional velocities are necessary to provide a Coriolis force to maintain the zonal velocity against viscosity and to provide enough heat convection to maintain the interior temperature field against conductive relaxation. The cause of the mean meridional flow of the wave is different and will be discussed in §§ 9 and 10.

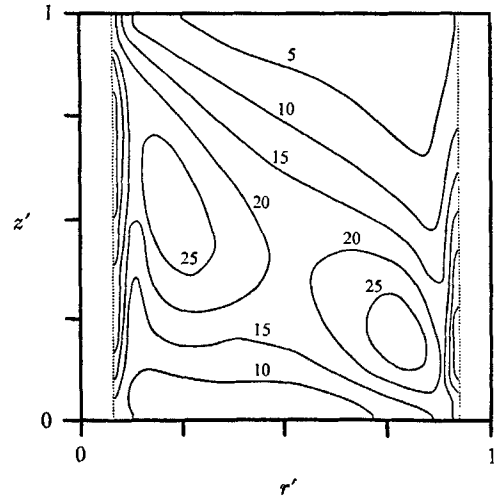

FIGURE 7. Baroclinicity of the interior region as given by $\bar{T}_r/\Delta T \times 10^2$.

The large differences between the axisymmetric state and the mean zonal state of the wave has important ramifications as regards constructing an analytical instability theory. This point will be discussed further in § 11 after the deviatoric fields have been examined.

7. The wave structure at $\Gamma' = \frac{1}{2}$

To obtain an immediate if not completely comprehensive idea of the nature of the wave we look at the deviatoric variables in the centre of the fluid, $r' = \frac{1}{2}$, as functions of height and azimuth (figure 8). For the u' variable, cross-sections at $r' = \frac{1}{4}$ and $\frac{3}{4}$ are displayed. These diagrams are indicative of the nature of the deviatoric field as will be seen in § 8. (The wave and total flow move to the right in these diagrams.)

This composite figure of the 5 basic deviatoric fields reveals what the annulus wave essentially is, namely a baroclinic wave similar to Eady's classical baroclinic wave, figure 9 (*b*). We can say this because the deviatoric fields have the same structure and inter-relationship between the variables as that of the theory, despite certain differences in their origins.

The relationship between the annulus wave solution and the theoretical Eady wave may be further displayed by abstracting from the solution a quasi-phase, amplitude figure. To do this heuristically the quasi-phase variation is based on the position of the zero value contours and the quasi-amplitude is derived by plotting the maximum, minimum values as functions of height. The results are shown in figure 9 (*a*). The resemblance to Eady's result is close despite the variations in shear and baroclinicity etc. present in the basic fields of the annulus. This figure displays the nucleus of the wave, establishing a link with analytical theory† that enables us to classify the solution.

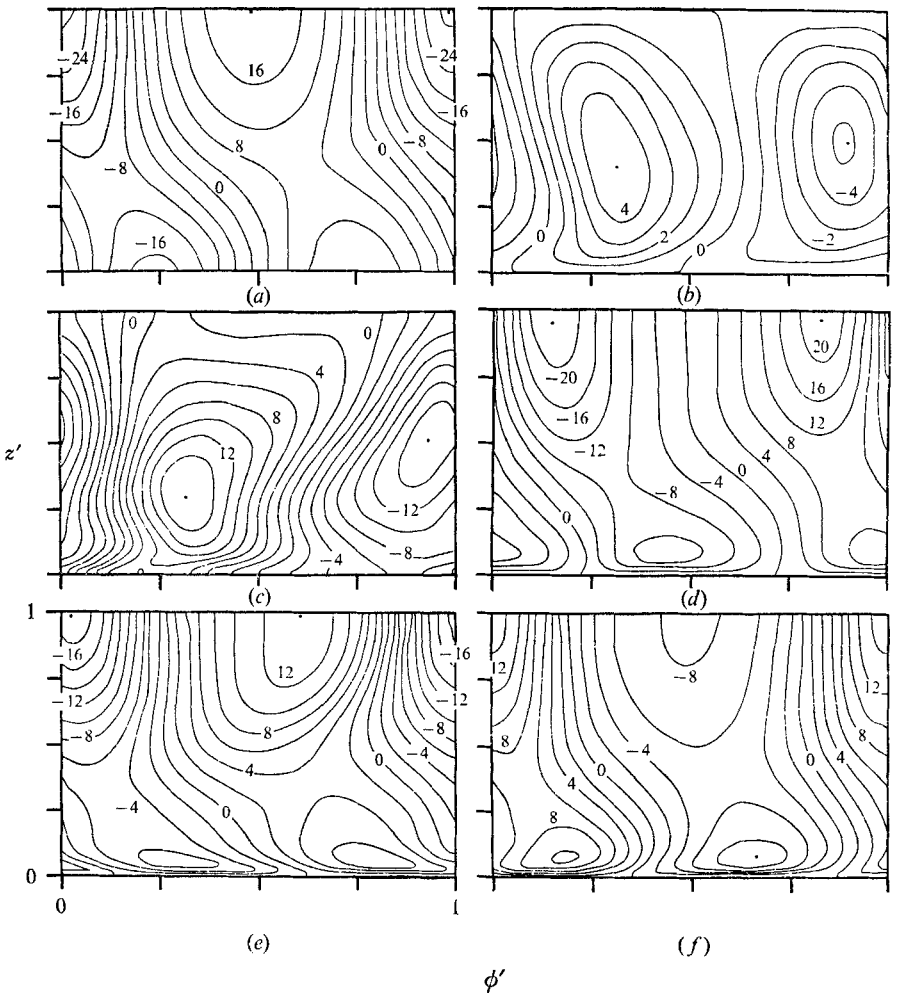

FIGURE 8. Composite of azimuthal sections of the deviatoric fields for the five basic variables (*a*) $(\pi' \times 10^2)$ cm^2 sec^{-2}, (*b*) $(w' \times 10^2)$ cm sec^{-1}, (*c*) $(T'/\Delta T \times 10^2)$, (*d*) $(v' \times 10^2)$ cm sec^{-1} at the centre of the fluid $r' = \frac{1}{2}$ and $(u' \times 10^2)$ cm sec^{-1} at (*e*) $r' = \frac{1}{4}$ and (*f*) $r' = \frac{3}{4}$. Ordinate is height z' and abscissa ϕ' over one wavelength. Diagrams are periodic in ϕ'.

† That also indicates that the solution is accurate.

The most significant deviation of the wave from Eady's solution occurs in the T' amplitude distribution. The annulus wave displays maximum T' values at mid-height whereas theory predicts minimum values at that level. This disagreement reflects the difference between the complex baroclinicity structure of the annulus (figure 7) and the simple structure of Eady's theory. Note, however, that the phase distributions of T' are similar.

The deviatoric fields of figure 8 are displayed in another way in figure 10 where all the variables at a given height are plotted as functions of azimuth, ϕ'. This form demonstrates the degree to which the fields vary sinusoidally. The diagrams at $z' = \frac{1}{4}, \frac{1}{2}, \frac{3}{4}$ represent the fluid interior, $z' = 1$ the free surface and $z' = \frac{1}{64}$ the Ekman layer. Thus diagram (*c*) for $z' = \frac{1}{2}$ represents the nearest the solution will come to the pure Eady wave.

The characteristics of this type of wave are well known. Briefly these are the tilting pressure wave, the geostrophically related v' wave with its phase shift of $\frac{1}{4}$ wavelength, and the in-phase w', T' waves with extrema at the middle level producing a strong release of potential energy. However, differences in the quasi-phase, amplitude distributions (figure 9 (*a*)) indicate some relatively moderate non-linear effects present in the annulus flow. The v' and w' waves are a $\frac{1}{2}$ wavelength out of phase with each other, the combined motion being upward and inwards toward the cold region and outward and downward toward the warm region.

The above picture of the wave structure of course represents only the central cylinder of fluid. We will show in the next section that a similar structure holds throughout much of the fluid. Although in the sidewall and Ekman boundary-layer regions the wave becomes modified, its overall behaviour is not significantly affected by the side layers. These layers remain essentially axisymmetric and interact very weakly with the interior wave, affecting it far less than does the base where a significant Ekman layer forms.

8. The complete wave structure

In this section flow behaviour over the whole fluid is examined. We are particularly interested in seeing how representative the Eady type structure at $r' = \frac{1}{2}$, discussed in § 7, is of the flow at other radii. The complete wave character could be determined by examining the various deviatoric distributions such as those in figure 8 throughout the fluid. This would be an intricate procedure and is not followed.

To obtain greater insight into the solution we construct quasi-phase, amplitude diagrams for all deviatoric variables as functions of r' and z' (figures 11 and 12). These figures form a two-dimensional extension of the simpler Eady figure and can be regarded as defining the nature of the wave. They perhaps form desirable invariants for annulus waves. This type of two-dimensional Eady figure for amplitude and phase was used by Eady (see Green 1970) and McIntyre (1970) to display results when lateral variations are introduced into the basic Eady problem. The distributions may also indicate the nature of certain solutions to the basic non-separable baroclinic instability problem.

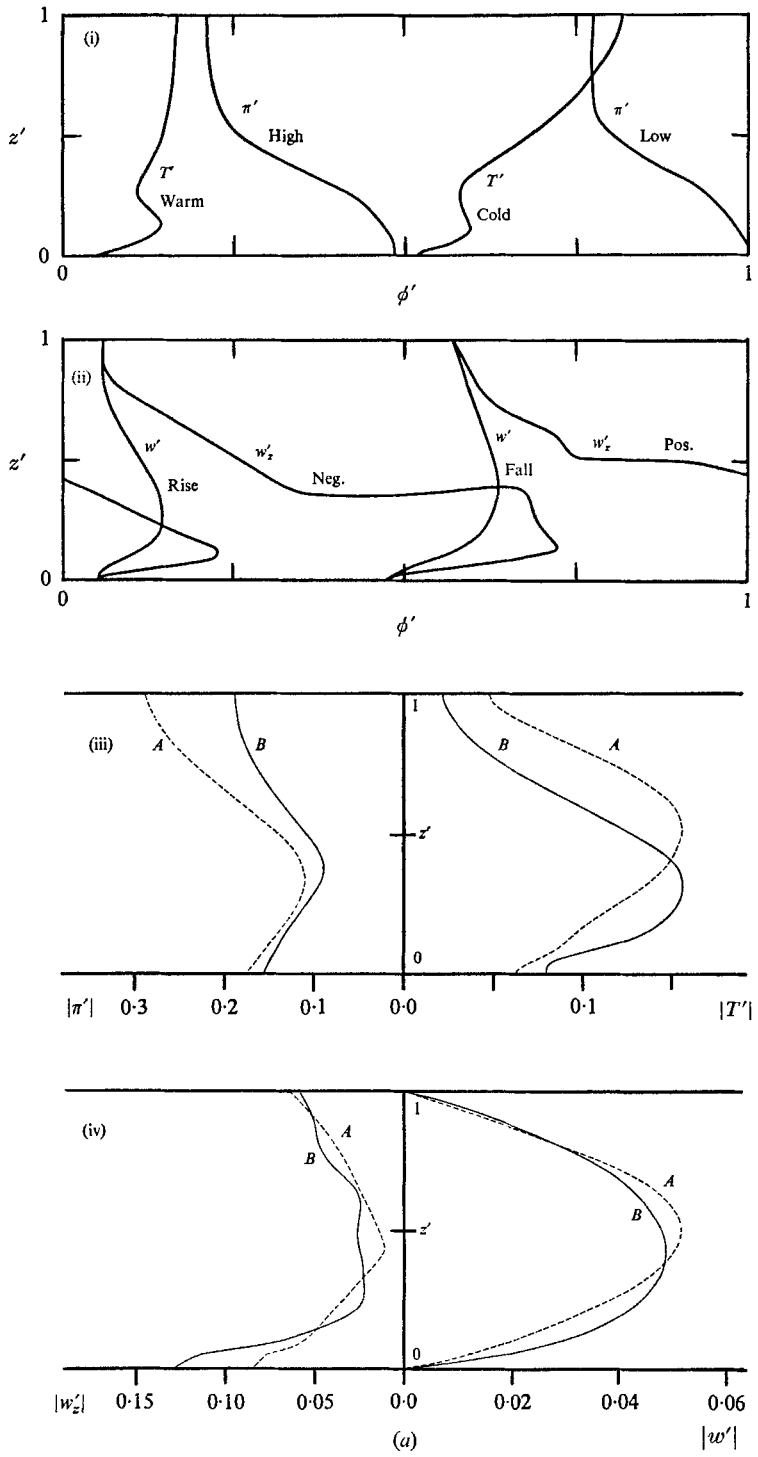

FIGURE 9. For legend see facing page.

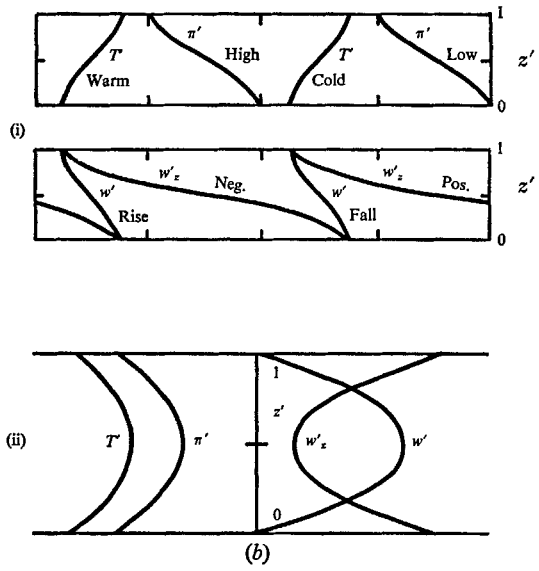

FIGURE 9. (*a*) Quasi phase and amplitude variations for the deviation fields π', T', w', w' of the wave solution at $r' = \frac{1}{2}$. Phases in diagrams (i) and (ii) are based on zero lines of figure 8 and amplitudes in diagrams (iii) and (iv) are based on the minimum, A, and maximum, B, values at given heights. Units are $cm^2\ sec^{-2}$ for π', cm sec^{-1} for velocities, sec^{-1} for w'_z.

(*b*) (i) Phases and (ii) amplitudes of an amplifying baroclinic wave on a linear u profile as given by Eady (1949). Compare with figure 9 (*a*). Labels such as 'high', 'warm' etc. describe regions to the right of the adjacent curve.

The quasi-phase, amplitude distributions are obtained by doing a Fourier analysis in the ϕ' direction. On retaining the coefficients of the first (and dominant) mode, the phase-amplitude diagrams can be constructed. Each phase is plotted relative to a reference value which is taken to be the maximum value in the interior at the top surface. The absolute phase values in reference to the pressure wave may be obtained by adding the phase shift constants.

Although the above procedure introduces an element of approximation into the analysis, the method is worthwhile because of the conciseness and insight achieved. The non-approximated three-dimensional wave features are given in Williams (1971). An examination of those figures indicates the validity of this approach and a comparison would perhaps help the reader visualize the actual distributions given by the somewhat abstract figures 11 and 12. The distributions at $r' = \frac{1}{2}$ in these figures contain much of the information given in the earlier diagrams of figures 8 and 9.

Overall, the quasi-amplitude patterns are smooth and well behaved, indicating the validity of this type of analysis. All the quasi-amplitudes, except u', have maxima near $r' = \frac{1}{2}$ and fall off toward the side boundaries. Again, all amplitudes except u' have all positive values. The π' quasi-amplitude resembles that given by Stone (1969), Eady (see Green 1970) and McIntyre (1970) for related problems. The v' quasi-amplitude pattern is very similar to that for π' (except in the Ekman layer) as are their respective quasi-phase distributions. This and

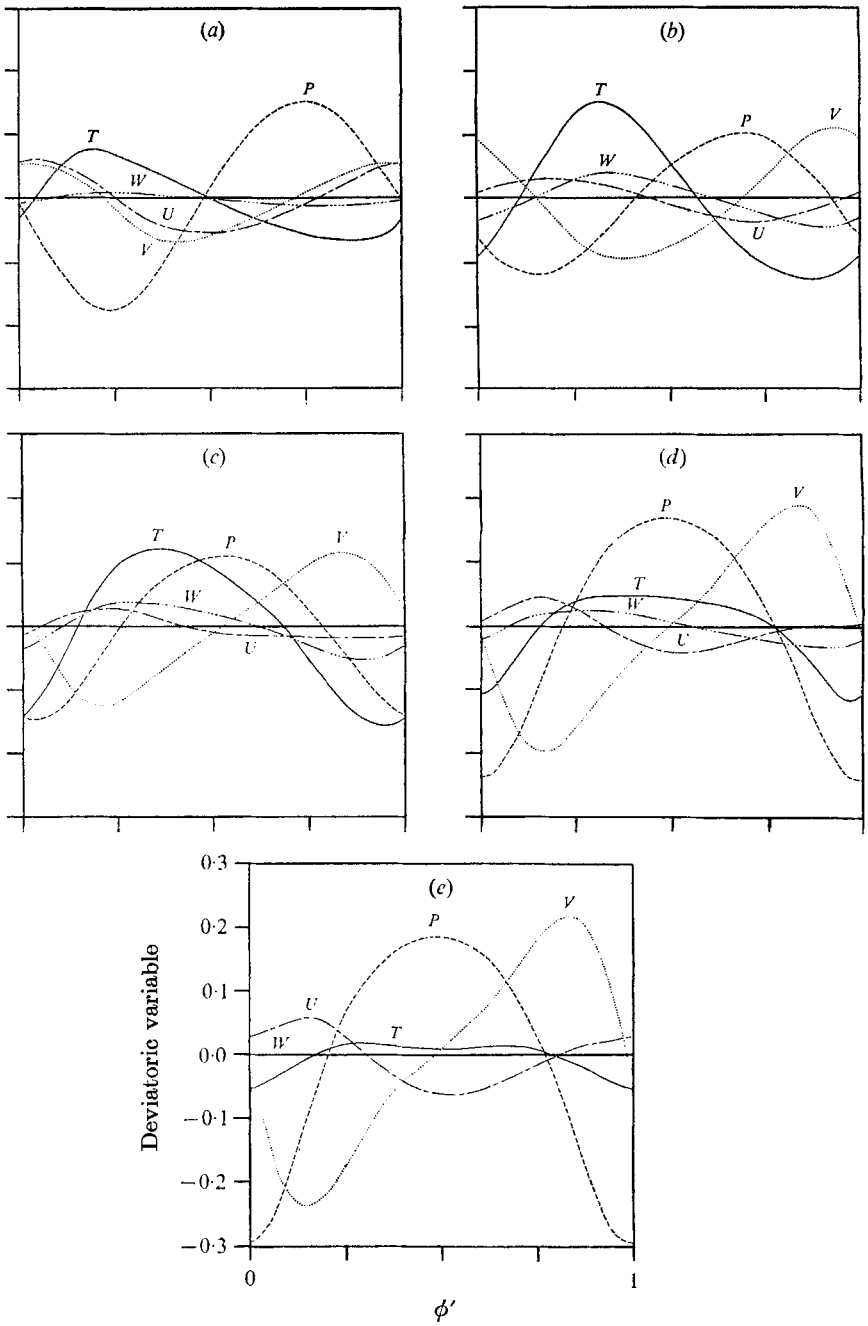

FIGURE 10. Deviatoric wave fields at $r' = \frac{1}{2}$ shown in amplitude verses azimuth form at different heights. The variables are (P) π' cm^2 sec^{-2}, (T) $T'/\Delta T$, (W) w' cm sec^{-1}, (U) u' cm sec^{-1} and (V) v' cm sec^{-1}. The heights are $z' =$: (a) $\frac{1}{64}$, (b) $\frac{17}{64}$, (c) $\frac{33}{64}$, (d) $\frac{49}{64}$, (e) $\frac{63}{64}$ (i.e. approximately $\frac{1}{4}$ intervals). Co-ordinates all as in (e).

the $\frac{1}{4}$ wavelength phase shift indicates a geostrophic relation between the two variables. Similarly the distribution of the quasi-phase and amplitude of u' are consistent with a partial geostrophic relation to π', except in boundary layers.

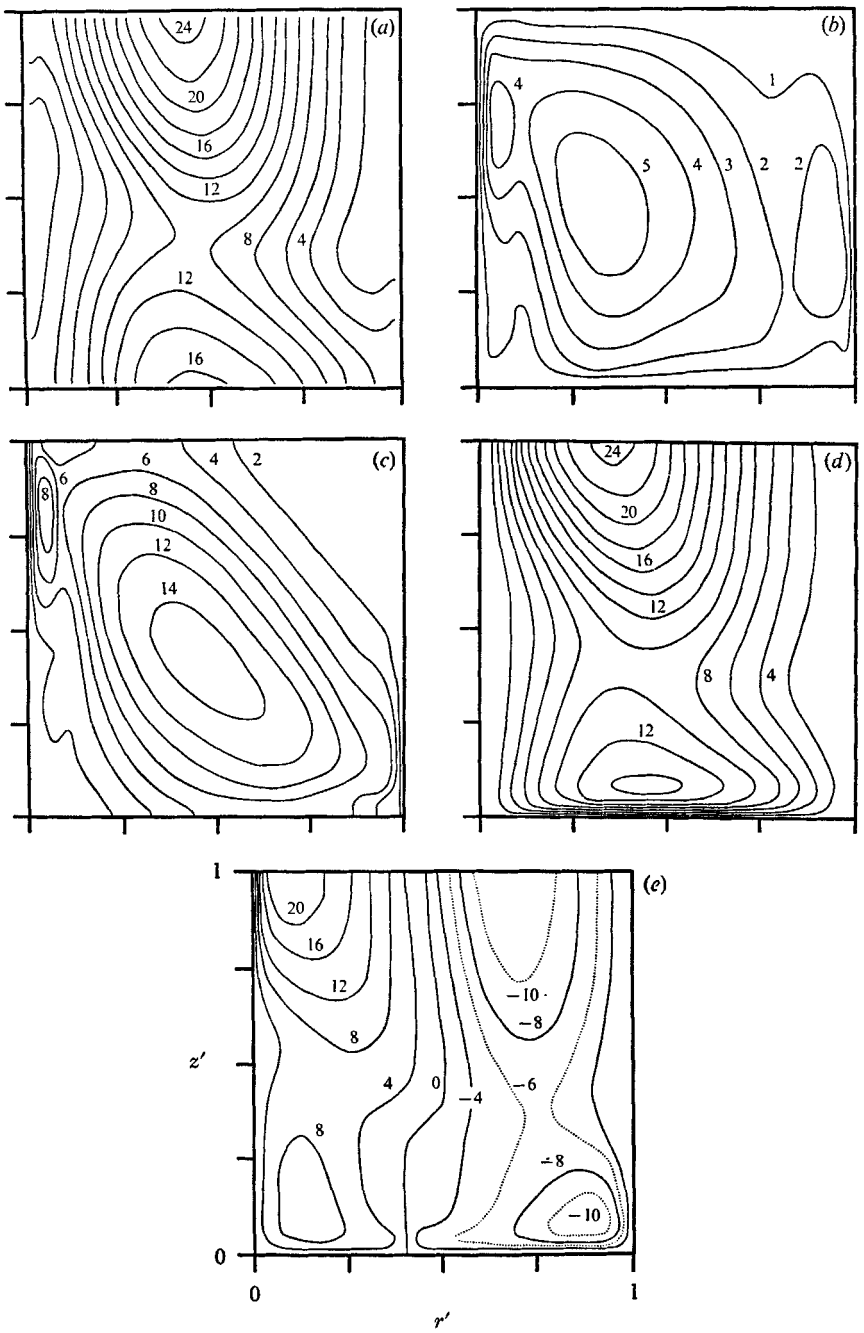

FIGURE 11. Quasi-amplitudes for the deviation fields of the wave solution. (*a*) ($\pi' \times 10^2$) cm^2 sec^{-2}, (*b*) ($w' \times 10^2$) cm^2 sec^{-1}, (*c*) ($T'/\Delta T \times 10^2$), (*d*) ($v' \times 10^2$) cm sec^{-1}, (*e*) ($u' \times 10^2$) cm sec^{-1}. Co-ordinates all as in (*e*).

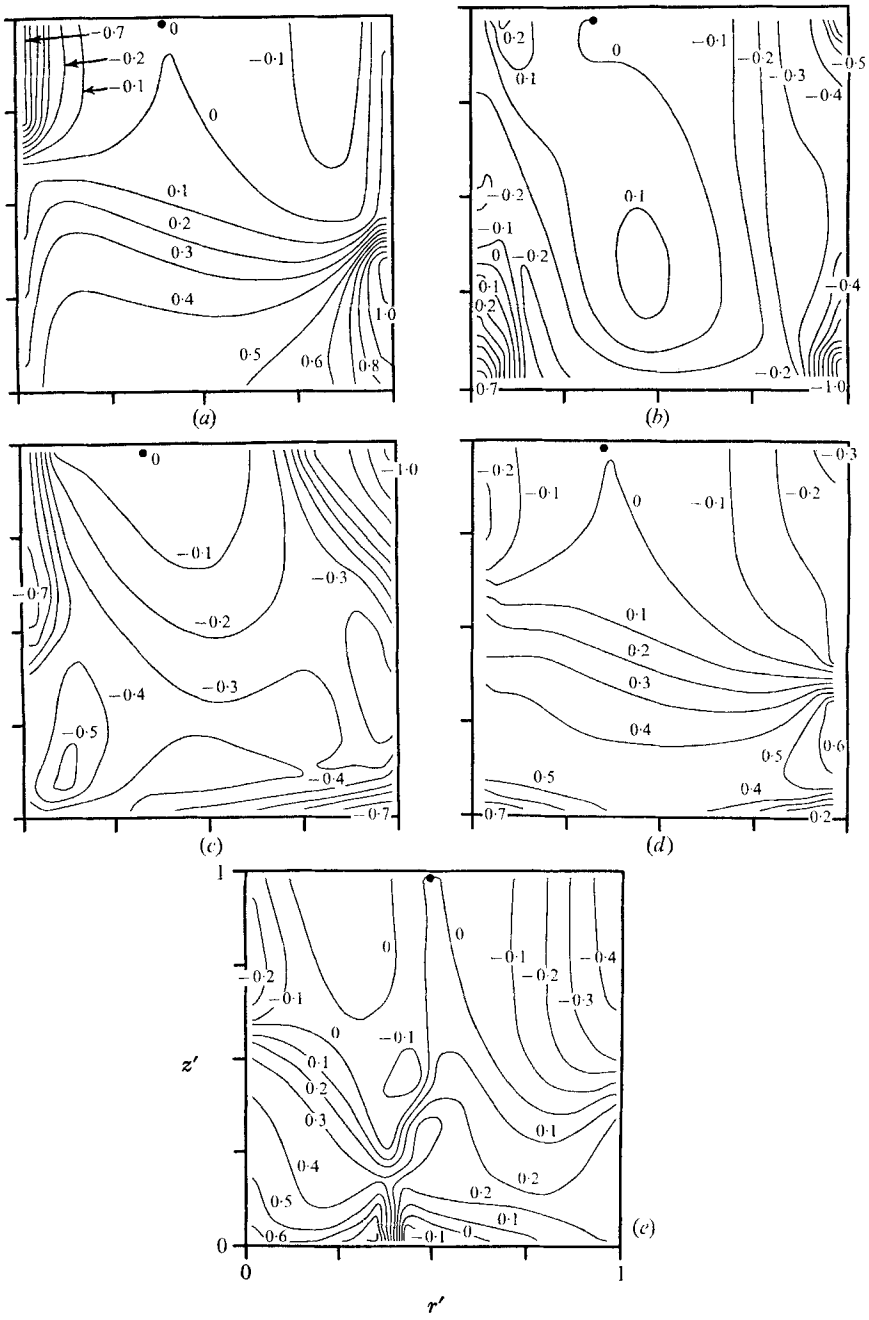

FIGURE 12. Quasi-negative relative phases for the deviation fields of the wave solution, for (*a*) π', (*b*) w', (*c*) T', (*d*) v', (*e*) u'. Negative phases are in units of π radians. Each diagram has phase drawn relative to maximum free surface value in the interior region, indicated by dot. To obtain absolute phase measured from π' field add the following constant phase shifts $c(T') = 0{\cdot}00$, $c(w') = -0{\cdot}35$, $c(v') = +0{\cdot}51$, $c(u') = +0{\cdot}02$. Co-ordinate all as in (*e*).

The quasi-amplitudes of w' and T' are similar in shape and the variables are closely in-phase, reflecting an efficient potential energy release. Some secondary side boundary-layer influences enter the w', T' amplitudes. The T' amplitude has a diagonally orientated axis, this being consistent with the baroclinicity field of figure 7.

In the negative phase diagrams, the notation is such that positive contour values indicate that the wave on that surface is ahead of the reference value. The negative phase lines of pressure, figure 12 (*a*), would be horizontal straight lines if the wave was a pure Eady wave. Clearly then variations in shear and baroclinicity affect the wave structure in the interior. The radial sloping of quasi-phase lines of π' indicates a transfer of angular momentum into the middle zone (except in the Ekman layer), see also § 10. In the boundary-layer regions on the sidewalls large variations in the π' phase occur. It has not been established that these variations are of physical significance, for in these regions the wave amplitude is weak and this type of analysis may not be valid. However, these diagrams may give some indication of what happens to the wave phase in boundary regions.

The quasi-negative phase of v' does not remain so closely geostrophically related to π' in the boundary-layer regions. The Ekman layer causes a retardation of the outer part of the v' wave but an advancement of the inner part in the base region. The Ekman layer has the same effect on the phase of the u' wave. The quasi-phase of u' is difficult to define near the centre of the base where the amplitude vanishes in a transition from positive to negative values.

The boundary and boundary-layer regions have a significant effect on the phase patterns of w' and T' in those regions. For the w' phase the strongest effects occur in the bottom corners and are associated with weak amplitudes. This effect may be seen in the basic w' field, Williams (1971), where at a given azimuth w' effectively changes sign at these corners from interior values. This may reflect a continuity requirement for the vertical flow of the central Ekman layer. In the T' phase pattern the concentrations are associated with weak amplitudes in the upper, outer region and with the thermal boundary layers on the sidewalls. All concentrations indicate a retardation of the T' wave.

The main conclusion that we can draw from figures 11 and 12 is that although a pure Eady wave is not present something closely related to it dominates the interior of the flow. Basically the wave is a baroclinic wave whose precise nature can only be defined by figures 11 and 12.

9. Energetic balance and transfer

The component terms of the prediction equations (1) to (4) show that the flow is essentially hydrostatic and geostrophic in the interior of the fluid (Williams 1971). In the vertical vorticity equation all terms, i.e. stretching, viscous diffusion, non-linear and time change appear to be significant. The presence of viscous diffusion in the vorticity equation might be expected as the balance is related to that of the axisymmetric u which has a known viscous term predominance (Williams 1967).

Figure 13 indicates schematically how the balance of the global energy

transfers defined by equations (11) to (13) is achieved. Both kinetic energy forms are maintained by conversion from potential energy, there being only a weak conversion from the deviatoric to mean kinetic energy. Thus the deviatoric wave gets its energy in the same way as the wave of inviscid, linearized theory and is essentially baroclinic. The magnitude of the deviatoric kinetic energy is about

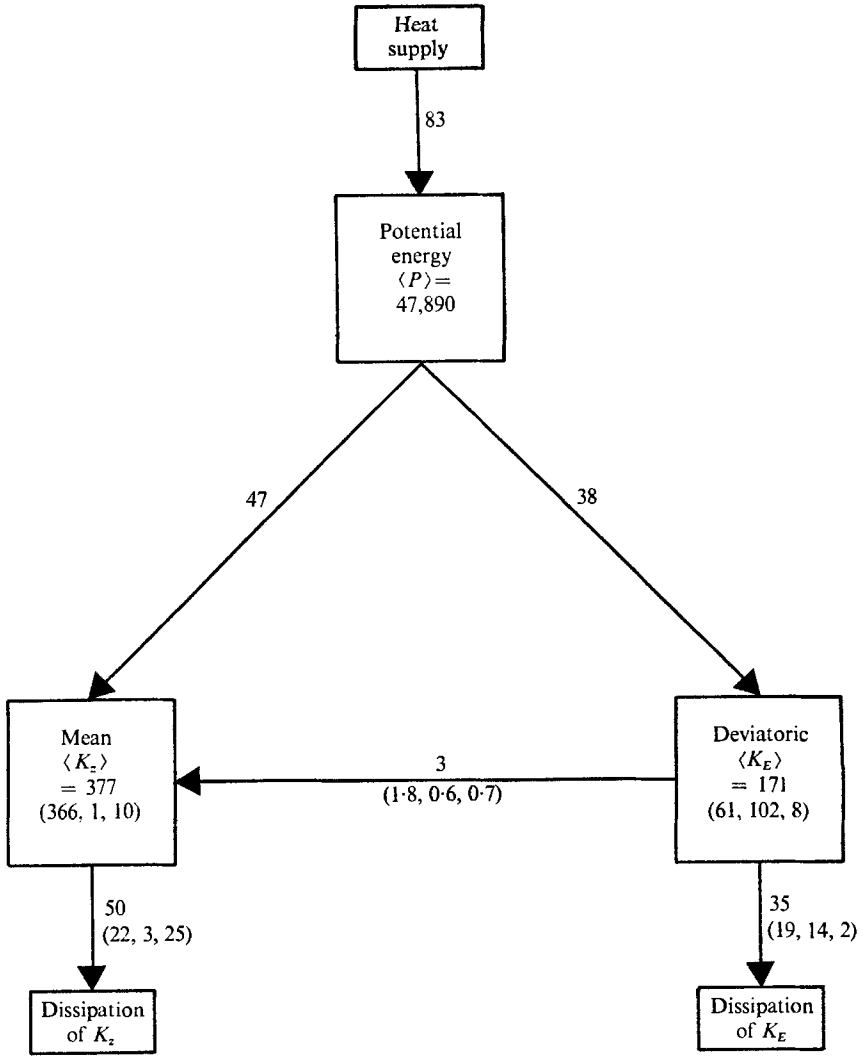

FIGURE 13. Schematic flow of energy from input at heat source to dissipation of kinetic energy. Integrals are over the wavelength volume and in units of 10^{-3} cm^5 sec^{-2} for the quantity terms and 10^{-3} cm^5 sec^{-3} for the conversions. Triads indicate contributions in the (u, v, w) components. Figure shows wave is baroclinic. Based on equations (11) to (15).

half that of the mean energy. The $\overline{v}$, $\overline{w}$ and w' components of the kinetic energy are all small. In the dissipation of mean kinetic energy the $\overline{w}$ component is large, reflecting the importance of vertical boundary layers in the mean flow. On the other hand in the deviatoric case the w' dissipation component is small indicating

that only weak vertical side boundary effects occur in the deviatoric flow. The opposite occurs in the Ekman layer with the $\bar{v}$, v' dissipation components being small and large respectively.

The role of the different boundary layers becomes more apparent when the local distribution of the kinetic energy sources and sinks are displayed (figure 14). The side boundary layers predominate in both the source and sink of the mean kinetic energy but in the deviatoric flow most of the energy comes from the interior region with only a minor contribution from the inner boundary layer. For the deviatoric flow the kinetic energy is dissipated in the Ekman layer and jet.

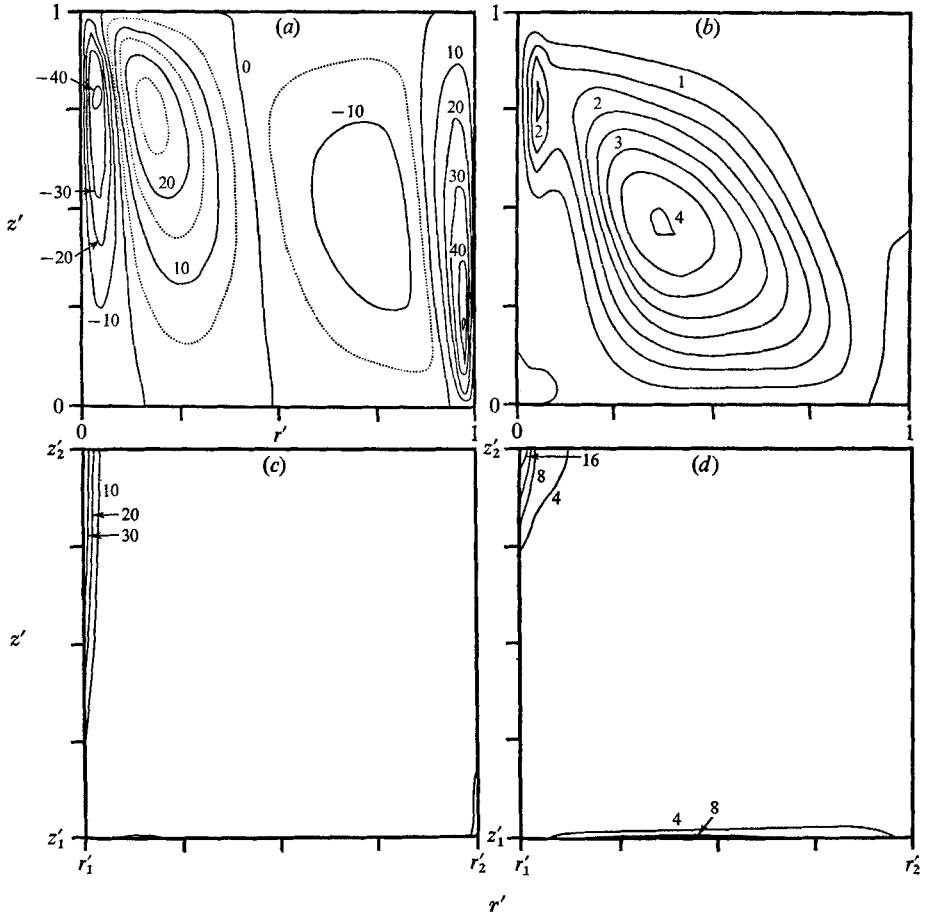

FIGURE 14. Local variation of energy sources and sinks (*a*) $\beta g\overline{\bar{w}\bar{T}}$ in 10^{-3} cm^2 sec^{-3}, (*b*) $\beta g\overline{w'T'}$ in 10^{-3} cm^2 sec^{-3}, (*c*) $\bar{\epsilon}^2$ in 10^{-3} cm^2 sec^{-3}, (*d*) $\overline{\epsilon'^2}$ in 10^{-3} cm^2 sec^{-3} from equations (22) and (23). The co-ordinates cover interior ranges r_1', $z_1' = \frac{1}{64}$ and r_2', $z_2' = \frac{63}{64}$.

Kinetic energy is created and destroyed in different regions of the fluid while the largest kinetic energy values occur at the free surface and to some extent in the Ekman layer (figure 15). Energy in the lowest quarter of the fluid is mostly deviatoric energy. The terms of equations (16) to (19), illustrated in figure 16, show how this energy system maintains itself. In both kinetic energy forms the

energy supply is transferred vertically from mid levels to upper and lower levels by the pressure interaction terms $(\overline{w}\overline{\pi})_z$ and $(\overline{w'\pi'})_z$ to balance the dissipation. An outstanding feature of the deviatoric energy balance of figure 16 (*b*) is the strong Ekman layer interaction in the wave through the deviatoric pressure field.

The pressure interaction term also dominates in the radial transfer of the mean kinetic energy and strong side-layer transfers are present. The slight imbalance between the terms shown in diagram (*c*) is made up by the transfers of the triple cell circulation.

In the radial transfer of the deviatoric kinetic energy, figure 16 (*d*), the side regions do not interact strongly with the interior. The small conversion from deviatoric to mean kinetic energy occurs at all radii. The net transfer due to the non-linear terms is small and the pressure interaction term seems to be the most effective transfer mechanism.

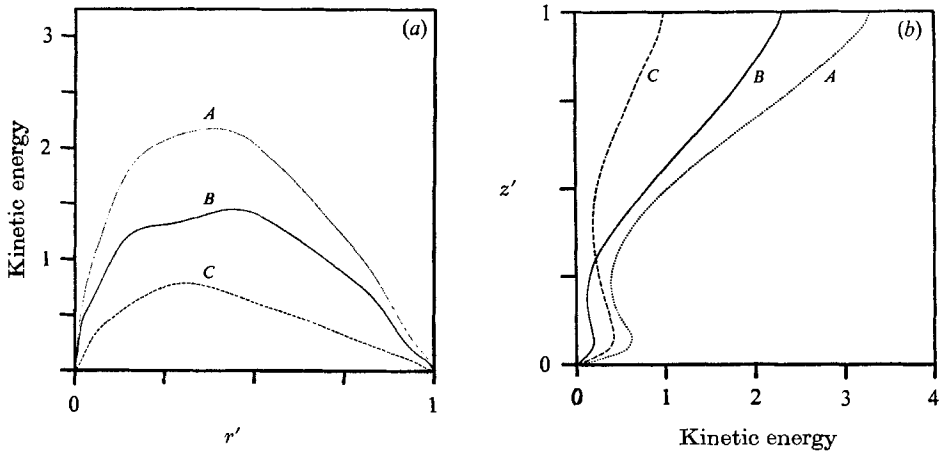

FIGURE 15. (*a*) Radial distribution of vertically averaged kinetic energies and (*b*) vertical distribution of radially averaged kinetic energies. (*A*) total, (*B*) mean, (*C*) deviatoric. Units 10^{-2} cm^2 sec^{-2}.

10. Angular momentum and heat balances

The maintenance of the mean temperature and zonal velocity fields and the associated role of the mean meridional circulation are most clearly demonstrated by the heat and angular momentum balances (figures 17 to 20). Each balance will be discussed separately and then the over-all functioning of the system will become apparent.

The boundary regions adjacent to the negative zonal flow form the source regions of angular momentum, the base being the major contributor. The remaining upper sections of the sidewalls form the main sinks of angular momentum, figure 17 (*a*). The momentum sink due to positive zonal flow in the mid-base region is smaller than the sidewall sinks but nonetheless is important to the dynamics of the interior region.

Both the mean circulation and deviatoric flow are active in the maintenance and transfer of the momentum source, sink system (figure 17). Cause and effect

being inseparable here we can only describe the consistency of the flow with the source, sink system it generates.

In discussing the angular momentum transfer it is convenient to consider the flow as being made up of 3 different regions, each one associated with a cell of the mean circulation. The mean meridional circulation at the sidewalls is responsible for transferring the angular momentum supplied by the base corner regions to

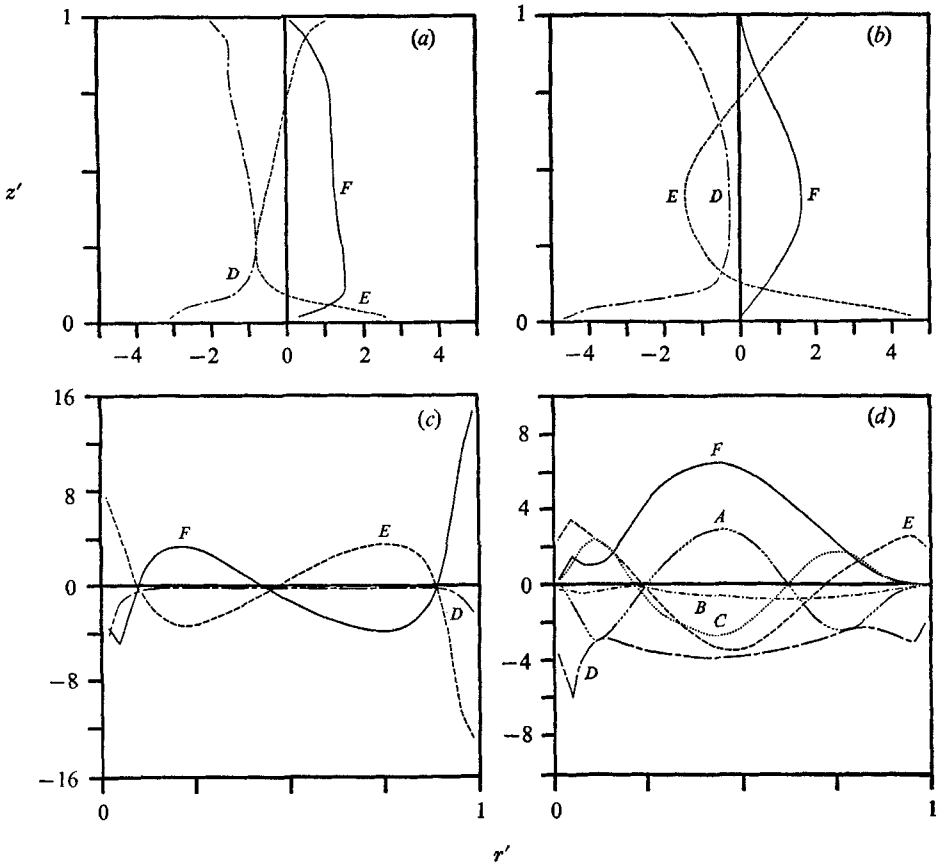

FIGURE 16. Top: vertical distribution of vertical kinetic energy balance for (*a*) mean energy and (*b*) deviatoric energy from equations (16) and (17). Below: radial distribution of radial kinetic energy transfer balance for (c) mean energy and (*d*) deviatoric energy from equations (18)–(19), multiplied by r for global comparison. Terms are (*A*) flux by total circulation, (*B*) conversion between deviatoric to mean energy, (*C*) interaction of deviatoric and mean energies, (*D*) viscous dissipation, (*E*) pressure interaction and (*F*) conversion from potential energy. Terms are negligible if not drawn. Units are 10^{-2} for (c), 10^{-3} for others, in $\mathrm{cm^2\ sec^{-3}}$.

higher levels where much of it is lost to the upper sidewalls, thereby maintaining the zonal flow against sidewall dissipation. Despite this dissipation the side regions produce a net supply of angular momentum. The deviatoric flux then acts to transport this supply into the axis of the angular momentum jet (figure 4 (*c*)) at $r' = \frac{1}{2}$ from both sides. Accumulation of angular momentum supply in

the jet is prevented by the central mean meriodional cell which acts in compensation to transfer momentum radially out of the jet and then to transport it downward to the central Ekman layer where it balances dissipation and maintains the positive zonal flow near mid-base.

The deviatoric transfer of angular momentum occurs largely in the upper levels and is generally against the gradient of the mean angular momentum field (although we note that the maximum angular momentum occurs slightly inward of the deviatoric flux maximum). Significant outward deviatoric transport occurs in the Ekman layer and figure 19 provides a closer look at the deviatoric angular momentum terms $\overline{ru'v'}$ and $\overline{ru'w'}$. The Ekman layer contribution to $\overline{ru'v'}$ can be reconstructed by superimposing the usual frictional cross-flow in and out of pressure centres methodically onto a simple geostrophic wave flow. The resulting flow forms the familiar sawtooth pattern characteristic of momentum transfer.

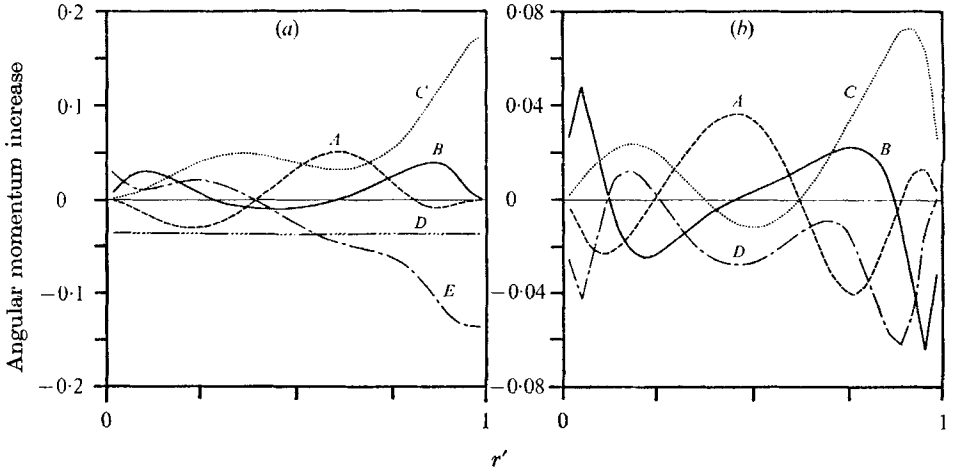

FIGURE 17. Radial distributions of radial angular momentum transfers (*a*) transport and maintenance of an inner ring: (*A*) eddy transport, (*B*) mean circulation transport, (*C*) torque at base, (*D*) torque at inner r = a cylinder, (*E*) torque at cylinder surface at r. Based on equation (26). (*b*) Transport and maintenance of mean angular momentum: (*A*) deviatoric flux, (*B*) mean circulation flux, (*C*) torque at base, (*D*) horizontal diffusion. Based on equation (25), the terms have been multiplied by r to allow for volume variation. Units are $cm^5\ sec^{-2}$ for (*a*) and $cm^3\ sec^{-2}$ for (*b*).

The above deviatoric momentum transfer is consistent with that obtained in the baroclinic instability theory of Pedlosky (1964), Stone (1969) and McIntyre (1970). These studies showed that baroclinic waves can produce deviatoric momentum transfers that tend to concentrate the jet and provide barotropic energy transfer toward the mean kinetic energy. For this to occur it is necessary to have lateral shear and that the wave be allowed to develop lateral phase variations, a feature not included in earlier instability studies. The lateral phase variations of the annulus wave (figure 12) are of course consistent with such deviatoric angular momentum transfers.

The main purpose of the annulus wave is of course to transfer heat and the terms of the mean temperature equation (27) show that this is accomplished in

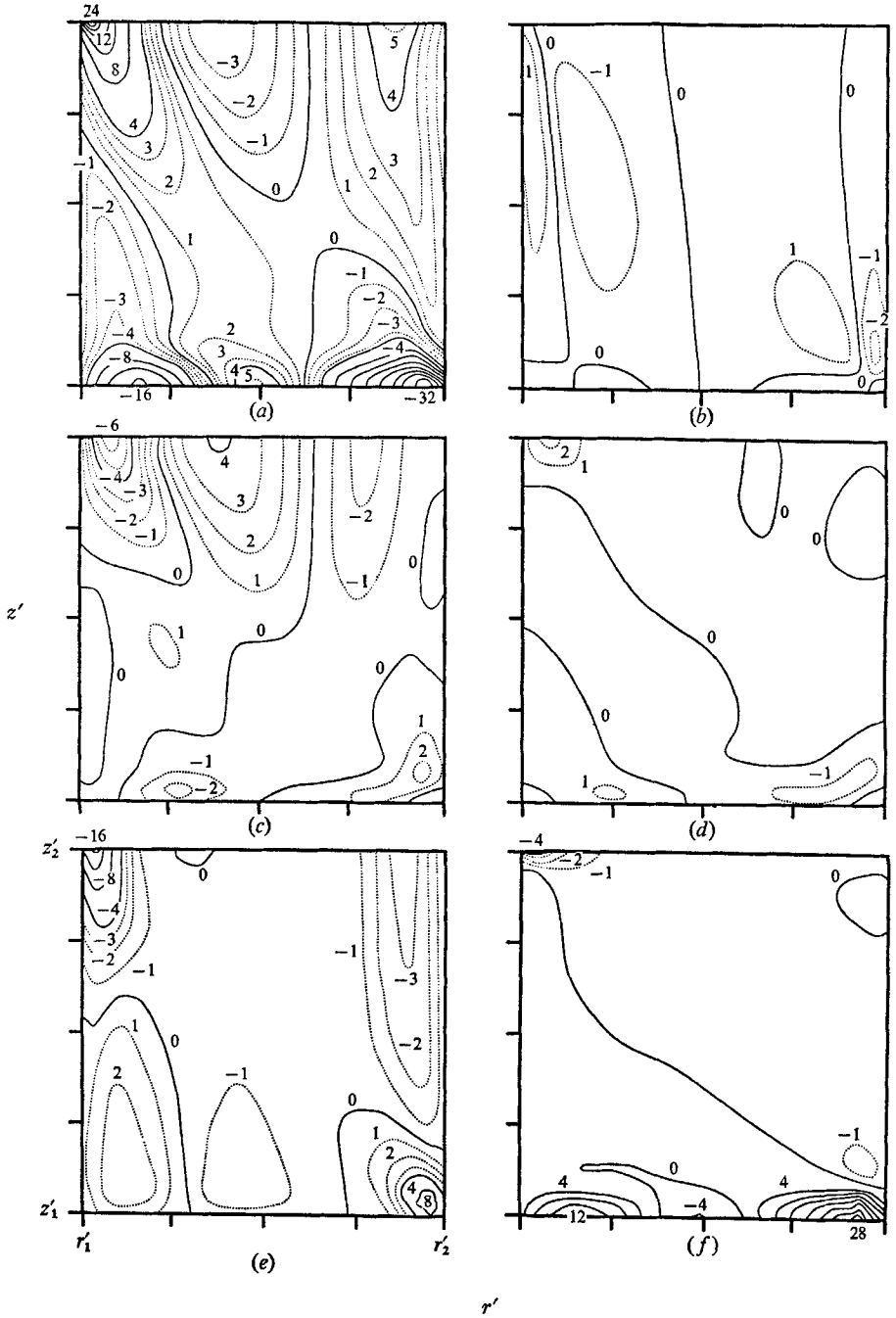

FIGURE 18. Components of the mean angular momentum equation (24). (*a*) $-\overline{v}\overline{m}_r$, (*b*) $-\overline{w}\overline{m}_z$, (*c*) $-1/r(r\overline{v'm'})_r$, (*d*) $-(\overline{w'm'})_z$, (*e*) $\nu r(\overline{m}_r/r)_r$, (*f*) $\nu\overline{m}_{zz}$. The co-ordinates cover the interior grid points of u, i.e. $r'_1, z'_1 = \frac{1}{64}$; $r'_2, z'_2 = \frac{63}{64}$. Units 10^{-2} cm^2 sec^{-2}. A reduced contouring interval is used for interior regions.

a relatively straightforward manner, figure 20. The mean meridional motion transports heat out of the outer side boundary layer into the adjacent region whence the deviatoric flow transports it across the fluid to the region adjacent to the inner boundary layer. There the mean circulation transfers it into the inner side boundary layer to be conducted into the inner cold wall.

The above angular momentum and heat balances demonstrate the consistency of the mean meridional circulation with the other mean fields in their mutual maintenance and co-existence. The two boundary-layer cells are needed to provide (*a*) the heat transfer to and from the side boundaries and (*b*) the momentum transfer from the base to the upper side boundaries for the maintenance of the zonal flow. The central cell is required for the momentum balance of the interior region and transfers momentum from the jet to the central Ekman layer.

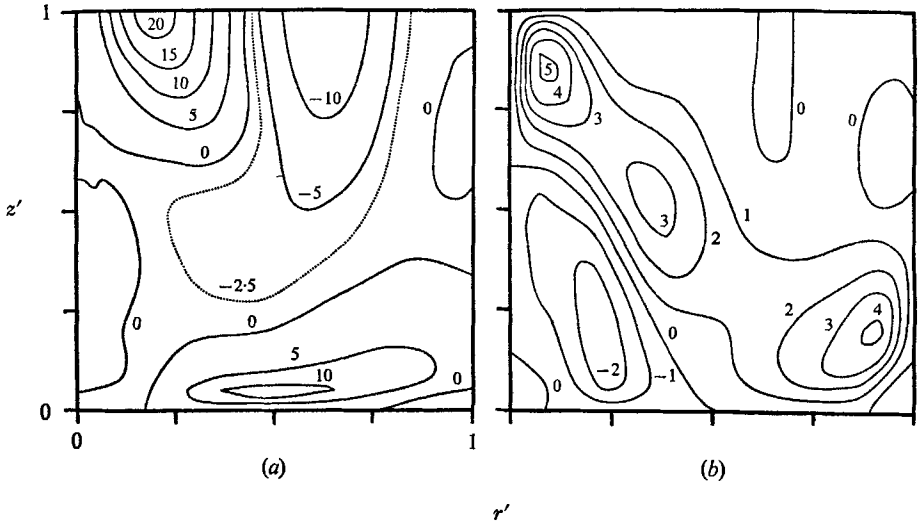

FIGURE 19. Deviatoric fluxes of angular momentum (*a*) $\overline{ru'v'}$ and (*b*) $\overline{ru'w'}$. Units are 10^{-3} cm^3 sec^{-2}.

11. Concluding summary

Detailed characteristics of the fluid mechanics of an annulus wave and of the axisymmetric flow at the same point in parameter space have been presented. The differences between these two solutions are fundamental.†

That the deviatoric wave motion is due to the baroclinic instability mechanism in the sense of Charney (1947) and Eady (1949) may be concluded from the kinematics and energetics, figures 8 to 13. The deviatoric wave resembles Eady's theoretical wave closely in the centre of the fluid and the complete wave can be defined in terms of two-dimensional quasi-phase, amplitude distributions (figures 11 and 12, § 8). Those diagrams also provide an indication of the form of baroclinic waves under the influence of lateral shear and baroclinicity variations and give an idea of the nature of certain solutions to the non-separable baroclinic instability problem.

† Lorenz (1970, § 5) gives a related discussion for the atmospheric system.

The separation of the wave solution into mean and deviatoric components revealed certain simple features, provided insight into the system and in so doing justified this method of analysis. A major characteristic of the deviatoric fields is the smallness of side boundary-layer features (figure 11). This is significant for it means that the complex features of the mean fields are not reproduced in the deviatoric fields. It also suggests that the wave primarily is a product of the interior region that is only slightly modified by the sidelayer regions. However,

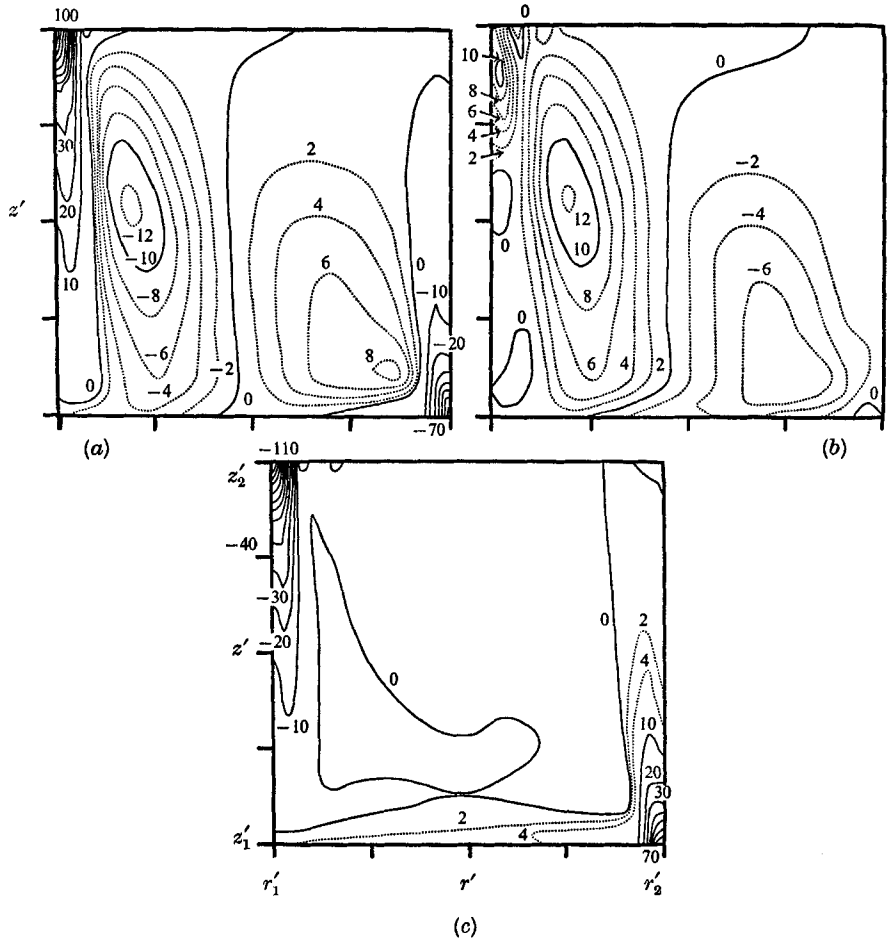

FIGURE 20. Components of the mean temperature equation (27). (*a*) Mean circulation flux $-[\bar{v}\bar{T}_r+\bar{w}\bar{T}_z]$, (*b*) deviatoric flux $-[(1/r)(\overline{rv'T'})_r+(\overline{w'T'})_z]$, (*c*) $\kappa\nabla^2\bar{T}$. Units are 10^{-3} sec^{-1}.

strong Ekman layer features are present and both the mean and deviatoric flows form strong Ekman layers. The importance of the Ekman layers in the deviatoric characteristics indicates why allowing for such layers in the analytical theory of annulus instabilities, Barcilon (1964), produces significant improvements in predicting the transition curve.

The large difference between the zonal mean state and the axisymmetric state points to a fundamental difficulty in our understanding of the wave and in

reconstructing it analytically. The disparity between the two states means that a linear baroclinic instability analysis of the axisymmetric state cannot explain the wave state. Only a non-linear analysis of a finite amplitude instability could provide this and that remains a difficult problem. The regularity of the deviatoric flow and its resemblance to waves produced by linear theory is deceptive for it may lead one to the conclusion that the zonal mean state is the proper mean state or the initial state of the stability analysis. This cannot be so for the basic mathematical requirements of stability theory demand that the initial state be a solution to the Navier–Stokes equations in the *absence* of the wave. It is possible that in finite amplitude the mean environment with which the wave interacts is the *wave-present* zonal mean state (and the character of the deviatoric fields suggest this). However it is not correct to regard the instability process as being the linear instability of the zonal mean state.

Turning to the geophysical implications of the solutions, a detailed comparison in every respect of the annulus dynamics with that of the atmosphere would not be relevant and would be extending the analogy beyond its intended limit. It is of interest however to draw attention to certain common characteristics of the two systems and this can be done most conveniently by comparing our figures with those of Smagorinsky *et al.* (1965). Such a comparison shows that although the mean fields are maintained by different mechanisms and although the atmospheric disturbances are not steady, there is a good similarity in the deviatoric (eddy) fields and transports. This could be taken as evidence in support of the view that many of the characteristic features of the atmosphere's dynamics and energetics simply reflect the finite amplitude consequences of baroclinic instability.

Comparison of the mean fields of the two systems however is another matter. Although there may be superficial resemblances the sources of potential energy in particular are different. In the atmosphere, radiative balance and latent heat of condensation are crucial. But the mean fields of the annulus are almost certainly influenced by the side boundary layers. This is true at least for the rigidly bounded axisymmetric case studied by McIntyre (1968) in which after accommodating a given Ekman transport, the thermal boundary layers approximately determine the average gradients of the interior temperature field. The balance of terms for our solution shows that the side boundary layers are sufficiently similar in nature for it to be reasonable to expect them still to be of considerable importance in maintaining the mean temperature.

How such a boundary layer influenced mean state and the associated deviatoric elements behave with variations in ΔT and Ω is not known and in any case cannot be compared with planetary atmospheres for which no ΔT is externally specified. Neither can the correspondence between the *effective* ΔT of the two systems be determined. Annulus convection has relevance to the basic studies of the baroclinic instability mechanism but remains a questionable analogue to planetary atmospheric motions.

I would like to thank Drs Syukuro Manabe and Michael McIntyre for detailed comments on this work and for suggestions that greatly helped the writing of

this paper. Discussions with Dr Isidoro Orlanski proved most valuable. I am also grateful to Dr Joseph Smagorinsky for the support that made this work possible. The meticulous drafting work of Mr Phillip Tunison is a greatly appreciated contribution.

REFERENCES

BARCILON, V. 1964 Role of Ekman layers in the stability of the symmetric regime obtained in a rotating annulus. *J. Atmos. Sci.* **21**, 291–9.

CHARNEY, J. G. 1947 The dynamics of long waves in a baroclinic westerly current. *J. Meteor.* **4**, 135–162.

EADY, E. T. 1949 Long waves and cyclone waves. *Tellus* **1**, 33–52.

FOWLIS, W. W. & HIDE, R. 1965 Thermal convection in a rotating annulus of liquid. *J. Atmos. Sci.* **22**, 541–558.

GREEN, J. S. A. 1970 Transfer properties of the large-scale eddies and general circulation of the atmosphere. *Quart. J. Roy. Met. Soc.* **96**, 157–185.

LORENZ, E. N. 1953 A proposed explanation for the existence of two regimes of flow in a rotating symmetrically-heated cylindrical vessel. *Proc. First Symp. on the use of Models in Geophys. Fluid Dyn.* pp. 73–80 (ed. R. R. Long). U.S. Govt. Printing Office.

LORENZ, E. N. 1962 Simplified dynamic equations applied to the rotating basin experiments. *J. Atmos. Sci.* **19**, 39–51.

LORENZ, E. N. 1963 The mechanics of vacillation. *J. Atmos. Sci.* **20**, 448–464.

LORENZ, E. N. 1967 The nature and theory of the general circulation of the atmosphere. *World Meteorological Organization.* Monograph no. 218, TP 115.

LORENZ, E. N. 1970 The nature of the global circulation of the atmosphere: a present view. *The Global Circulation of the Atmosphere* (ed. G. A. Corby), pp. 3–23. Royal Met. Society.

MCINTYRE, M. E. 1968 The axisymmetric convective regime for a rigidly bounded rotating annulus. *J. Fluid Mech.* **32**, 625–655.

MCINTYRE, M. E. 1970 On the non-separable baroclinic parallel flow instability problem. *J. Fluid Mech.* **40**, 273–306.

PEDLOSKY, J. 1964 The stability of currents in the atmosphere and the ocean: Parts I and II. *J. Atmos. Sci.* **21**, 201–219, 342–353.

PEDLOSKY, J. 1970 Finite-amplitude baroclinic waves. *J. Atmos. Sci.* **27**, 15–30.

SMAGORINSKY, J., MANABE, S. & HOLLOWAY, J. L. 1965 Numerical results from a nine-level general circulation model of the atmosphere. *Mon. Weath. Rev.* **93**, 727–768.

STONE, P. H. 1969 The meridional structure of baroclinic waves. *J. Atmos. Sci.* **26**, 376–389.

WILLIAMS, G. P. 1967 Thermal convection in a rotating fluid annulus. Parts 1 and 2. *J. Atmos. Sci.* **24**, 144–161, 162–174.

WILLIAMS, G. P. 1969 Numerical integration of the three-dimensional Navier–Stokes equations for incompressible flow. *J. Fluid Mech.* **37**, 727–750.

WILLIAMS, G. P. 1971 The synoptic nature of an annulus wave. *Mon. Weath. Rev.* (in the Press).